Molecular Pharmacology Fast Forward. Published on April 19, 2013 as doi:10.1124/mol.113.085670

EXPLORATION OF THE ORTHOSTERIC/ALLOSTERIC INTERFACE IN HUMAN M1 MUSCARINIC RECEPTORS BY BITOPIC FLUORESCENT LIGANDS

Sandrine B. Daval, Esther Kellenberger, Dominique Bonnet, Valérie Utard, Jean-Luc Galzi and Brigitte Ilien

Unité Biotechnologie et Signalisation Cellulaire, UMR 7242 CNRS, LabEx Medalis, Université de Strasbourg, Illkirch, France (S.D., V.U., JL.G., B.I.); Laboratoire d'Innovation Thérapeutique, UMR 7200 CNRS, Université de Strasbourg, Illkirch, France (E.K., D.B.)

Molecular Pharmacology Fast Forward. Published on April 19, 2013 as DOI: 10.1124/mol.113.085670
This article has not been copyedited and formatted. The final version may differ from this version.

Running title : Bitopic poses of fluorescent BoPz ligands on M1 receptors

Corresponding author :

Dr Brigitte ILIEN

Unité Biotechnologie et Signalisation cellulaire, UMR 7242 CNRS, Université de Strasbourg

Ecole Supérieure de Biotechnologie de Strasbourg

300 Bvd S. Brant - BP 10413

67412 Illkirch (France)

Phone : +33 3 68 85 47 38 ; Fax : +33 3 68 85 46 83 ; Email : brigitte.ilien@unistra.fr

Number of text pages : 40 (including references)
Number of tables : 5
Number of figures : 7
Number of references : 57
Number of words in Abstract : 238
Number of words in Introduction : 731
Number of words in Discussion : 1505
Supporting information : 3 Figures (S1-S2-S3) and 1 Table.

Abbreviations: ACh, acetylcholine; ATCM, allosteric ternary complex model; mAChR, muscarinic cholinergic receptor; hM1, human M1 muscarinic receptor; ecl, extracellular loop; EGFP, Enhanced Green Fluorescent Protein; HEK, human embryonic kidney; FRET, Fluorescence Resonance Energy Transfer; Bodipy, boron-dipyrromethene; Pz, pirenzepine; BoPz, Bodipy pirenzepine; NMS, N-methylscopolamine; PBS, phosphate buffer saline; QNB, 3-quinuclidinyl benzilate; TM, transmembrane domain.

Molecular Pharmacology Fast Forward. Published on April 19, 2013 as DOI: 10.1124/mol.113.085670
This article has not been copyedited and formatted. The final version may differ from this version.

ABSTRACT

Bitopic binding properties apply to a variety of muscarinic compounds that span and simultaneously bind to both the orthosteric and allosteric receptor sites. We provide evidence that fluorescent pirenzepine derivatives, with the M1 antagonist fused to the Bodipy [558/568] fluorophore via spacers of varying lengths, exhibit orthosteric/allosteric binding properties at muscarinic M1 receptors. This behaviour was inferred from a combination of functional, radioligand and FRET binding experiments, performed under equilibrium and kinetic conditions on EGFP-fused M1 receptors. Though displaying a common orthosteric component, the fluorescent compounds inherit bitopic properties from a linker-guided positioning of their Bodipy moiety within the M1 allosteric vestibule. Depending on linker length, the fluorophore is allowed to reach neighbouring allosteric domains, overlapping or not with the classical gallamine site, but distinct from the allosteric indocarbazolole 'WIN' site. Site-directed mutagenesis, as well as molecular modeling and ligand docking studies based on recently solved muscarinic receptor structures, further support the definition of two groups of Bodipy-pirenzepine derivatives exhibiting distinct allosteric binding poses. Thus, the linker may dictate pharmacological outcomes for bitopic molecules that are hardly predictable from the properties of individual orthosteric and allosteric building blocks. Our findings also demonstrate that the fusion of a fluorophore to an orthosteric ligand is not neutral as it may confer, unless carefully controlled, unexpected properties to the resultant fluorescent tracer. Altogether, this study illustrates the importance of a 'multifacette' experimental approach to unravel and validate bitopic ligand binding mechanisms.

Molecular Pharmacology Fast Forward. Published on April 19, 2013 as DOI: 10.1124/mol.113.085670
This article has not been copyedited and formatted. The final version may differ from this version.

INTRODUCTION

The five muscarinic receptor subtypes (mAChRs; M1-M5) play prominent roles in the central and parasympathetic nervous systems and are potential therapeutic targets (Eglen 2012). Decades of research have enriched a wide collection of high affinity and efficacious molecules competing with the neurotransmitter ACh for binding to muscarinic receptors. Unfortunately, most of these agonists and antagonists lack true subtype selectivity, a drawback related to the conservation of the orthosteric binding site across mAChRs. Thus, drug discovery programs shifted to the development of allosteric compounds targeting topographically distinct and less conserved binding sites (May et al., 2007; De Amici et al., 2009).

A number of allosteric modulators and agonists now provide useful tools to finely tune orthosteric ligand affinity and efficacy at muscarinic receptors, to select subsets of signalling or regulatory pathways, and to mediate subtype-selective functional outcomes (Birdsall and Lazareno, 2005; Gregory et al., 2007; Conn et al., 2009; Digby et al., 2010). The molecular interpretation of functional versatility and its exploitation in drug discovery are still very challenging as one has to consider the ability of every compound, or combination of allosteric partners, to stabilize discrete conformational and functional receptor states within a given cell context (Kenakin and Miller, 2010; Deupi and Kobilka, 2010; Gregory et al., 2012). The recent resolution of M2 (Haga et al., 2012) and M3 (Kruse et al., 2012) receptor structures confirmed the close proximity of allosteric and orthosteric sites and the possibility for orthosteric antagonists to pause at an allosteric site while associating to and dissociating from the receptors (Jakubik et al., 2000; Redka et al., 2008; Ilien et al., 2009). Such features may explain the difficulty to define the molecular mechanisms (allosteric transition versus steric hindrance) underlying the effects of muscarinic allosteric compounds (Proska and Tucek 1994; Canals et al., 2012) and the persistent observation of hybrid properties for several molecules. Indeed, orthosteric antagonists, such as pirenzepine derivatives (Tränkle et al.,

1998; Ellis and Seidenberg 1999; Lanzafame et al., 2001) and methoctramine (Giraldo et al., 1988), as well as 'allosteric' agonists like McN-A-343 (Valant et al., 2008), xanomeline (Jakubik et al., 2002) and AC-42 derivatives (Avlani et al., 2010; Gregory et al., 2010; Daval et al., 2012) most probably inherit subtype-dependent affinity or efficacy patterns from mixed orthosteric/allosteric binding properties.

Hybrid, dualsteric or bitopic compounds form an emerging class of molecules aiming at major improvements in affinity, efficacy and functional selectivity through the combination (via a spacer arm) of orthosteric and allosteric building blocks (Mohr et al., 2010, Valant et al., 2012). Proof-of-concept of the bitopic strategy has been done by dissecting the partial muscarinic agonist McN-A-343 into an orthosteric and an allosteric fragment whose combination allowed to recapitulate the pharmacology of the parent molecule (Valant et al., 2008). Pioneering *de novo* design of dualsteric molecules has been accomplished on the M2 receptor too, with the description of molecules combining a non selective orthosteric antagonist (Steinfeld et al., 2007) or agonist (Disingrini et al., 2006; Antony et al., 2009 ; Bock et al., 2012) with M2-preferring allosteric moieties. Binding and functional experiments indicated that such hybrids may indeed display better subtype-selectivity, improved affinity (antagonist hybrids) or stimulus-biased (agonist hybrids) signalling properties.

We previously reported on the synthesis and similar nanomolar affinity at muscarinic M1 receptors of a family (BoPz) of Bodipy pirenzepine derivatives, differing by the length (10 to 22 atoms) of the linker connecting the Bodipy[558/568] fluorophore to the M1-selective antagonist (Tahtaoui et al., 2004). Fluorescence resonance energy transfer (FRET) studies performed on EGFP-fused M1 muscarinic receptors suggested the existence of two groups of molecules on the basis of linker length, donor (EGFP) – acceptor (Bodipy) distance in ligand-receptor complexes and allosteric modulation. We proposed a bitopic binding mode

for the Bo(15-22)Pz series of ligands, with their fluorophore and pirenzepine moieties exploring allosteric and orthosteric receptor domains, respectively.

In the present work, we undertook a systematic characterization of all BoPz members to get a better knowledge on the orthosteric and allosteric partners (receptor sites and ligand moieties) involved in their interaction with M1 receptors. In order to validate true bitopic binding mechanisms, these ligands were taken as 'competitors' (functional and [^{3}H]-NMS assays) and as fluorescent tracers (FRET studies) and compared for their behaviour under equilibrium and kinetic conditions. Topographical information on the receptor domains recruited by these fluorescent derivatives was essentially from the examination of ^{M1}Trp400 (7.35) and ^{M1}Trp405 (7.40) receptor mutants and molecular modeling.

Molecular Pharmacology Fast Forward. Published on April 19, 2013 as DOI: 10.1124/mol.113.085670
This article has not been copyedited and formatted. The final version may differ from this version.

MATERIALS AND METHODS

Materials. [^{3}H]-N-Methyl scopolamine chloride ([^{3}H]-NMS ; 65 Ci/mmol) was from Perkin Elmer Life and Analytical Sciences (Courtaboeuf, France). Atropine sulfate, NMS bromide, pirenzepine dihydrochloride, acetylcholine chloride, carbachol chloride, gallamine triethiodide, brucine sulfate, staurosporine and WIN 51,708 hydrate were purchased from Sigma-Aldrich (Saint-Quentin Fallavier, France). Bodipy[558/568] pirenzepine hydrochloride (referred to as Bo(10)Pz in this paper) and Indo-1 acetoxymethyl ester were from Molecular Probes (Invitrogen, Cergy Pontoise, France).

Chemistry. Bo(12)Pz, Bo(15)Pz and Bo(22)Pz fluorescent pirenzepine derivatives, together with the Bo(5) compound, were synthesized as reported (Tahtaoui et al., 2004). Their purity was checked by analytical RP-HPLC. Absorbance and fluorescence spectroscopic properties were examined using a Cary 1E (Varian) photometer and a Spex Fluorolog 2 (Horiba Jobin-Yvon, Longjumeau, France) fluorimeter. The chemical structures of fluorescent derivatives and of other compounds used throughout this study are presented in Figure 1.

EGFP-fused muscarinic M1 receptors, mutagenesis and cell expression. The human M1 muscarinic receptor with a truncated N terminus (deletion of 17 amino acids) fused to EGFP is the construct of reference defined as EGFP(Δ17)hM1 (Ilien et al., 2003). The corresponding cDNA served as a template in polymerase chain reaction to get single point-mutated M1 receptors at tryptophan residues 400 and 405. Using the QuickChange™ site-directed mutagenesis kit (Stratagene, Amsterdam, The Netherlands), Ala or Phe residues were inserted in place of Trp by addition of synthetic oligonucleotide primers containing the required triplet changes. Following subcloning into the pCEP4 expression vector (Invitrogen, Cergy Pontoise, France) and extraction of the plasmids using the Qiagen® Plasmid Midi kit (Qiagen, Courtaboeuf, France), the mutations were finally confirmed by sequencing.

Molecular Pharmacology Fast Forward. Published on April 19, 2013 as DOI: 10.1124/mol.113.085670
This article has not been copyedited and formatted. The final version may differ from this version.

HEK cells were transfected with wild-type (EGFP(Δ17)hM1) or mutant (referred to as EGFP-W400A/F and EGFP-W405A/F) plasmids by calcium phosphate precipitation and selected with 2 mg/mL hygromycin-B (Eurobio, Courtaboeuf, France) for stable receptor expression.

Cell culture. IMR 32 human neuroblastoma cells and human embryonic kidney HEK 293 cells (American Type Culture Collection; LGC Promochem, Molsheim, France) were grown at 37°C in a 5% CO_2 humidified atmosphere in Dulbecco's modified Eagle's medium (DMEM) and in minimal essential medium (MEM with 2 mM glutamine), respectively. Both media (Gibco, Fisher Scientific, Illkirch, France) were supplemented with 10% fetal calf serum, penicillin (100 U/mL) and streptomycin (100 µg/mL). Nearly confluent cells were harvested by mild 0.05% trypsin/0.02% EDTA (w/v) or Versene (PBS with 5 mM EDTA) treatment, counted, washed twice by centrifugation before final resuspension in physiological Hepes buffer (10 mM HEPES, 0.4 mM NaH_2PO_4, 137.5 mM NaCl, 1.25 mM $MgCl_2$, 1.25 mM $CaCl_2$, 6 mM KCl, 10 mM glucose and 1 mg/mL bovine serum albumin, pH 7.4). Cell suspensions were kept on ice until further use in binding assays.

Calcium mobilization assays. Adherent cells (either non transfected or stably expressing various M1 receptor constructs) were loaded with 5 µM Indo-1/AM for 40 min at 37°C, harvested by rapid trypsin/EDTA treatment, washed, and finally suspended (10^6 cells per mL) in Hepes buffer. Agonist-evoked increases in intracellular calcium were recorded over time at 20°C through fluorescence emission at 400 nm (excitation at 338 nm). Cells were pre-incubated for 10 min with antagonists before agonist challenge. Peak amplitudes were normalized to basal and maximal (cells permeabilized with 20 µM digitonine) fluorescence levels and expressed as a percentage of the maximal control response.

Radioligand binding assays. [^{3}H]-NMS binding assays were conducted in Hepes buffer using 30,000 (EGFP-W405F), 60,000 (EGFP(Δ17)hM1, EGFP-W400F and EGFP-W405A) or 100,000 (EGFP-W400A) HEK cells per assay. Equilibrium binding experiments

Molecular Pharmacology Fast Forward. Published on April 19, 2013 as DOI: 10.1124/mol.113.085670
This article has not been copyedited and formatted. The final version may differ from this version.

proceeded in the presence of 0.1 nM [^{3}H]-NMS (unless otherwise stated) and of various concentrations of unlabelled ligands, in a 1 mL final volume. Incubation lasted for 22 h at 20°C and was terminated by filtration through Whatman GF/B glass fibre filters (presoaked in 0.2% polyethyleneimine) positioned on a Brandel cell harvester (Alpha Biotech, London, UK). Tubes and filters were rinsed three times with 3 mL ice-cold 25 mM Tris-HCl buffer (pH 7.4). Radioactivity on filters was counted by liquid scintillation spectrometry. Specific [^{3}H]-NMS binding was defined as the difference between total and non specific binding measured in the presence of 4 µM atropine.

Off-rate assays were performed according to a 'three time point dilution and blocking' procedure (adapted from Lazareno et al., 1995). A 100-fold concentrated cell suspension was pre-incubated for 30 min at 25°C with 3 nM [^{3}H]-NMS, in the absence (total binding) or the presence (non specific binding) of 10 µM atropine, then kept on ice. 10 µL aliquots of both pre-labelled cell batches were added to a series of test tubes filled with 1 mL Hepes buffer (at 25°C) containing 10 µM atropine alone or combined with other drugs at various concentrations. At three given dissociation time points, the reaction was stopped by rapid filtration as described above. Specific [^{3}H]-NMS binding at equilibrium was assessed in parallel through direct filtration of undiluted 10 µL labelled cell samples and radioactivity counting.

FRET monitoring of BoPz binding to EGFP-fused M1 receptors. Fluorescence data were acquired from living cells suspended in Hepes buffer (1 to 3 10^6 cells /mL, depending on receptor expression) and kept at 20°C in a thermostated quartz cuvette under magnetic stirring. The interaction of BoPz tracers with chimeric M1 receptors was followed as a variation in cell fluorescence intensity (recorded at 510 nm) due to resonance energy transfer from the EGFP donor (excited at 470 nm) toward the ligand Bodipy acceptor species (Ilien et al. 2003, 2009).

Molecular Pharmacology Fast Forward. Published on April 19, 2013 as DOI: 10.1124/mol.113.085670
This article has not been copyedited and formatted. The final version may differ from this version.

Equilibrium binding studies, which require the parallel treatment of large series of samples, were conducted in a manner very similar to radioligand binding experiments. Cells were incubated in test tubes for 22 h at 20°C with the fluorescent tracer and unlabelled drugs (1 mL final volume). As FRET assays do not require separation of free from bound tracer, binding levels were quantified through simple fluorescence readouts at 510 nm (excitation at 470 nm). Association and dissociation kinetics were followed in real time as described (Tahtaoui et al., 2004; Ilien et al., 2009). Briefly, recordings of fluorescence intensity started with the addition of 4 µL of fluorescent ligand (250-fold concentrated DMSO stock) to the 1-mL cell suspension (pre-incubated or not at 20°C with various compounds) and lasted until binding equilibrium was confirmed by visual inspection of the stability of the fluorescence trace. Thereafter, dissociation of ligand-receptor complexes was initiated by adding 10 µM atropine (or any combination of unlabelled drugs; 'isotopic' dilution protocol) to the incubation medium and fluorescence was recorded over time until full recovery. An alternate 'volumetric' dilution protocol was applied as follows : the 1 mL incubation was cooled down at 4°C, centrifuged for 20 sec at 1,500 g, and the supernatant was carefully removed. The tiny cell pellet was rapidly resuspended in 1 mL Hepes buffer (20°C; supplemented or not with 10 µM atropine) and immediately monitored for fluorescence recovery over time.

Specific binding of BoPz derivatives to EGFP-fused hM1 receptors was defined, under equilibrium binding conditions, as the difference in fluorescence intensity of cells incubated with the tracer, in the absence or the presence of a saturating concentration of atropine. Under kinetic conditions, specific binding was derived from the amplitude of tracer-induced fluorescence extinction (association step) or of atropine-promoted fluorescence recovery (dissociation step). Theoretically, both determinations should define an identical FRET signal amplitude. When using high tracer concentrations or colored compounds, samples were

Molecular Pharmacology Fast Forward. Published on April 19, 2013 as DOI: 10.1124/mol.113.085670
This article has not been copyedited and formatted. The final version may differ from this version.

systematically checked (and corrected) for possible interferences with cell fluorescence measurements.

Homology modeling. The structure of the human muscarinic M1 receptor (UNIPROT: ACM1_human) was obtained by homology to the rat muscarinic M3 receptor (PDB: 4daj, chain A). Sequence alignment and homology modeling were performed using MOE 2011 (Chemical Computing Group Inc., Montreal, Canada). The disulfide bonds were automatically detected. For each receptor, a maximum of 10 models were constructed independently for the main chain, and a single set of side chains was then built for each main chain model. The models were refined by tethered minimization and ranked according to Coulomb and generalized Born interaction energies. The top ranked model was further refined by energy minimization. The AMBER99 forcefield was used for all energy calculations.

Docking of ligands into the M1 receptor. The three-dimensional structures of brucine, gallamine, pirenzepine and its fluorescent BoPz derivatives were generated using Corina 3.1 (Molecular Network GmbH, Erlangen, Germany). An ensemble of 63 conformers was generated for pirenzepine using Omega 2.4.3 (OpenEye, Inc., Santa-Fe, CA, U.S.A.). Each conformer was compared to the tiotropium-bound M3 structure (PDB: 4daj, Chain A) using ROCS 3.2.1 (OpenEye, Inc., Santa-Fe, CA, U.S.A.). The best matched conformer, which yielded a CombSoscore of 1.27, was pasted into the M1 model and the resulting complex was refined by energy minimization using MOE.

Brucine, gallamine and BoPz compounds were individually docked into the M1 receptor using GOLD 5.1 (Cambridge Crystallographic Data Centre, Cambridge, UK). The boron atom of Bodipy was replaced with a carbon atom, because boron is not supported by the docking program. The M1 binding pocket was defined as all protein residues located in a 16Å-radius sphere centered on the CZ atom of Tyr404. Docking of brucine and gallamine was performed with the default settings of the program. Docking of each BoPz derivative was performed with

Molecular Pharmacology Fast Forward. Published on April 19, 2013 as DOI: 10.1124/mol.113.085670
This article has not been copyedited and formatted. The final version may differ from this version.

the parameters of the genetic algorithm preset for 10,000 operations, and was biased with constraints on the pirenzepine moiety (constraints on donors, acceptors and on shape, with weight set to 10) and on the linker (hydrophobic atoms preferentially placed in a 2.5Å sphere centered on the mass center defined by the 6-membered rings of Tyr82, Trp101 and Tyr404). BoPz poses not reproducing the reference binding mode of pirenzepine were filtered using the in house IFP program (Marcou and Rognan 2007). Bodipy positioning in the M1 7TM core was then explored by manually modifying the rotatable bonds in the linker using Sybyl-X1.3 (Tripos, Inc., St. Louis, MO, U.S.A.).

Data analyses. Nonlinear regression analyses of functional and binding data were performed using Kaleidagraph 4.0 (Synergy software, Reading, PA, USA).

Occupancy curves were generated by plotting the signal amplitude Y, as a function of agonist or tracer concentration X, and analyzed according to the empirical Hill Equation :

$$Y = Y_{max} / (1 + (L_{0.5} / [X])^{nH})) \quad (1)$$

where Y_{max} is either the maximal response E_{max} for an agonist, the maximal number B_{max} of binding sites for a radioactive tracer, or the maximal amplitude of fluorescence extinction F_{max} at saturating concentrations of a fluorescent tracer. $L_{0.5}$ is the agonist concentration EC_{50} leading to half-maximal response or the apparent equilibrium dissociation constant K_d for tracer binding. n_H is the midpoint slope.

Antagonist-induced rightward shifts of occupancy curves were checked for competitive interaction using Lew and Angus (1995) equation :

$$pL_{0.5} = - \log ([B]^s + 10^{-pK}) - \log c \quad (2)$$

where $pL_{0.5}$ is the negative logarithm of agonist $EC_{50,obs}$ or tracer K_{app} values measured at each antagonist concentration [B]. pK and log c are fitting constants, s is the Schild slope.

Curve shifts were also analyzed according to Arunlakshana and Schild (1959) equation :

$$\log (DR-1) = s \cdot \log [B] - \log K \quad (3)$$

Molecular Pharmacology Fast Forward. Published on April 19, 2013 as DOI: 10.1124/mol.113.085670
This article has not been copyedited and formatted. The final version may differ from this version.

where dose-ratios DR ($EC_{50,obs}$ / $EC_{50,control}$ or K_{app} / $K_{d,control}$) serve to quantify midpoint shifts at each antagonist concentration [B]. K is an estimate of antagonist potency and s is the Schild slope. If not significantly deviating from unity, the s value was constrained as such in Eqs. 2 and 3 and K represented the affinity constant K_b for a competitive antagonist. Otherwise, a pA_2 value was estimated via the pA_2 = pK/s relationship. Functional antagonism associated with depression of maximal responses was also analysed, as reported (Christopoulos et al., 1999), using equi-effective agonist EC_{25} values (leading to a constant level of response equal to 25 % of the maximal control response) as the dependent variable in Eqs. 2 or 3.

Data from competition-type binding experiments were expressed as B/B_0 ratios, with B_0 and B referring to specific tracer binding at equilibrium, in the absence and the presence of an unlabelled competitor, respectively. Fractional receptor occupancy B/B_0 was plotted against the concentration of competitor [X] and analysed using the mass-action equation :

$$B/ B_0 = Bottom + [(Top-Bottom) /(1 + (IC_{50} / [X])^{nH})] \quad (4)$$

where 'Top' and 'Bottom' parameters refer respectively to the upper and lower plateau values of the curve, IC_{50} denotes the X-value at the inflection point and n_H is the slope factor.

IC_{50} values of compounds that led to "full displacement" at high concentrations (Bottom and slope values non significantly different from 0 and 1, respectively), whatever the tracer concentration, were converted into equilibrium dissociation constants K_i using the Cheng and Prusoff relationship for a competitive interaction. In case of submaximal inhibition (Bottom > 0; $B/B_0 \leq 1$) or binding potentiation (Bottom = 1; $B/B_0 \geq 1$), data were fitted to the allosteric ternary complex model (ATCM; Ehlert 1988; Lazareno et al., 1995) :

$$B/B_0 = ([L] + K_d) / ([L] + K_d \cdot [(1 + [X] / K_x) / (1 + [X] / \alpha.K_x)]) \quad (5)$$

where [L] and [X] are the concentrations of tracer and allosteric agent, respectively. K_d and K_x denote the equilibrium dissociation constants of the tracer and the alloster at the free receptor, respectively. The cooperativity factor α denotes the magnitude by which the

Molecular Pharmacology Fast Forward. Published on April 19, 2013 as DOI: 10.1124/mol.113.085670
This article has not been copyedited and formatted. The final version may differ from this version.

equilibrium dissociation constants of either ligand to its site is modified (α >1: negative cooperativity; α <1: positive cooperativity) by the concomittant presence of the other ligand. In case of nearly neutral cooperativity (α close to 1), an allosteric ligand weakly impacts tracer binding at equilibrium and curve fitting using Eq. 5 does not work. Assuming the equivalence of $\alpha.K_x$ and $EC_{50,diss}$ (see below) parameters to define the affinity of an allosteric agent for tracer-occupied receptors (Raasch et al., 2002), α was replaced by $EC_{50,diss}/K_x$ in Eq. 5 and the remaining variable K_x was obtained from curve fit. The cooperativity factor α was then derived from the $EC_{50,diss}/K_x$ ratio.

Biphasic binding kinetics, as afforded from real-time monitoring of the association of fluorescent ligands to EGFP-fused M1 receptors or of the dissociation of Bo(10)Pz from the EGFP-W405A mutant, were analysed by fitting individual traces to a two-exponential model :

$$F(t) = A_0 + A_1 . \exp^{(-k1 . t)} + A_2 . \exp^{(-k2 . t)} \quad (6)$$

where A_1 and A_2 are the amplitudes of fluorescence changes associated with the rapid and slow components, A_0 is the fluorescence intensity at infinite time t. Depending on the experimental paradigm, k_1 and k_2 denote either apparent association rate constants or off-rate constants for the fast and slow events, respectively.

Unless otherwise stated, all dissociation kinetics for [^{3}H]-NMS or BoPz tracers from wild-type or mutant receptors, when examined in the absence or the presence of allosteric agents, followed a monoexponential time course reaction :

$$B_t = B_0 . \exp^{(-koff . t)} \quad (7)$$

where B_0 and B_t represent specific binding at equilibrium and at dissociation time t, respectively. k_{off} denotes the tracer dissociation rate constant.

Concentration-effect curves for the allosteric delay of tracer dissociation were generated by plotting $k_{off,obs}$ / $k_{off,control}$ ratios (i.e. off-rate constants measured in the presence or the absence of an allosteric agent) as a function of [X], the alloster concentration. Fitting to Eq. 8 :

Molecular Pharmacology Fast Forward. Published on April 19, 2013 as DOI: 10.1124/mol.113.085670
This article has not been copyedited and formatted. The final version may differ from this version.

$$k_{off}\ obs\ /\ k_{off}\ control = Bottom + [(1\text{-}Bottom)\ /(1 + (EC_{50,diss}\ /\ [X])^{nH})] \quad (8)$$

allowed the determination of the alloster concentration $EC_{50,diss}$ leading to half-maximal reduction of control tracer off-rate, the amplitude $E_{max,diss}$ (1-Bottom value) of the retardation effect and the slope factor n_H. If not significantly different from unity, n_H was constrained as such and the $EC_{50,diss}$ parameter was taken as an estimate of the equilibrium affinity constant of the allosteric modulator at tracer-occupied receptors.

Molecular Pharmacology Fast Forward. Published on April 19, 2013 as DOI: 10.1124/mol.113.085670
This article has not been copyedited and formatted. The final version may differ from this version.

RESULTS

The members of the BoPz family (Fig. 1) display two typical building blocks, i.e. the pirenzepine (Pz) pharmacophore and the Bodipy (Bo) [558/568] fluorophore, connected via spacers of varying length (10 to 22 atoms) and nature (isopeptidic or PEG type). The Bo(5) compound, with a short aliphatic chain, lacks the pirenzepine moiety.

Along with their first description (Tahtaoui et al., 2004), BoPz derivatives have been suspected to divide into two separate Bo(10,12)Pz and Bo(15,22)Pz groups. To further explore the properties of all these ligands, a number of experiments have been conducted and will be illustrated with selected members of each putative group.

Functional antagonism by BoPz derivatives of M1-mediated calcium mobilization

We first examined the ability of EGFP(Δ17)hM1-expressing HEK cells to adequately report on allosteric modulation of M1-mediated responses to ACh. Brucine and gallamine were taken as compounds of reference (Fig. 1) as they are known to positively and negatively tune, respectively, ACh affinity and potency at M1 receptors (Birdsall et al., 1999; Birdsall and Lazareno, 2005). The presence of endogenous muscarinic M3 receptors in HEK cells was found to introduce bias in the modulation of ACh-induced calcium signals in EGFP(Δ17)hM1-expressing HEK cells (Supplemental Fig. S1). In contrast, IMR 32 neuroblastoma cells, which are deprived of M3 sites and elicit a clear M1-mediated calcium response to muscarinic agonists (Heikkilä et al. 1991), allowed the observation of brucine and gallamine properties in agreement with their modulatory roles on M1 receptor function. Therefore, IMR 32 cells were selected as an useful companion system to EGFP(Δ17)hM1 cells to examine, from a functional point of view, the nature of Bo(10)Pz, Bo(15)Pz and pirenzepine interaction with M1 receptors.

As shown in Figure 2, increasing concentrations (nanomolar to micromolar range) of all three compounds promote a dextral shift of dose-response curves together with a profound

Molecular Pharmacology Fast Forward. Published on April 19, 2013 as DOI: 10.1124/mol.113.085670
This article has not been copyedited and formatted. The final version may differ from this version.

depression in agonist maximal response, both in EGFP(Δ17)hM1 (top panel) and in IMR 32 (lower panel) cells. Often taken as a hallmark for non competitive inhibitors, insurmountable antagonism for orthosteric antagonists is widespread across a range of receptor systems and assays (Kenakin et al., 2006), including pirenzepine effects on muscarinic responses in various cell lines (Christopoulos et al. 1999 and references therein). A common explanation is to consider that a slowly dissociating antagonist, the agonist and the receptor cannot come to proper equilibrium in fast responding systems, thereby limiting maximal response amplitude. Such kinetic artefacts most probably apply to pirenzepine, Bo(10)Pz and Bo(15)Pz inhibition of transient calcium responses in both cell lines. Indeed, they slowly dissociate from M1 receptors with off rate constants ($sec^{-1} \times 10^{-4}$) close to 5 for pirenzepine (Potter et al., 1989; Mohr and Trankle 1994; Christopoulos et al., 1999) and in the range of 5 to 15 for BoPz derivatives (Table 5). One should add too that BoPz compounds, at the lowest concentrations which were tested, probably did not reach true equilibrium when pre-incubated with cells for 10 min.

Potency estimates for insurmountable antagonists can be obtained with no prior knowledge of molecular mechanism through pA_2 measurements (Kenakin et al., 2006). Lew and Angus (1995) as well as Arunlakshana and Schild (1959) analyses (Fig. 2 right) favoured the hypothesis of a competitive interplay of the antagonists with ACh (slope factors not significantly different from 1). The pA_2 values for Bo(10)Pz (7.98 ± 0.29; 8.15 ± 0.22), Bo(15)Pz (8.10 ± 0.21; 7.95 ± 0.23) and pirenzepine (7.89 ± 0.10; 7.77 ± 0.25) antagonism in EGFP(Δ17)hM1 and IMR 32 cells, respectively, were consistent with their binding affinity constants determined from FRET and [^{3}H]-NMS studies (Tables 1 and 2). Regression analyses using equi-effective agonist concentrations (EC_{25} values) instead of standard EC_{50} values provided similar potency estimates (not shown). Thus, these functional experiments aiming at defining the competitive or non competitive interplay of BoPz antagonists with ACh remained non decisive.

Molecular Pharmacology Fast Forward. Published on April 19, 2013 as DOI: 10.1124/mol.113.085670
This article has not been copyedited and formatted. The final version may differ from this version.

FRET studies : Kinetic insights into BoPz binding at EGFP(Δ17)hM1 receptors.

Given the ideal acceptor property of the Bodipy [558/568] fluorophore for energy transfer from excited EGFP, BoPz compounds have proven valuable FRET probes to dissect ligand binding mechanisms at EGFP(Δ17)hM1 receptors (Ilien et al. 2003, 2009; Tahtaoui et al. 2004). Figure 3 depicts real-time recordings of association and dissociation processes for BoPz tracers and the impact of allosteric modulators (brucine and gallamine) on their kinetics. Top and bottom panels refer to BoPz probes with short and long linkers, respectively.

Preincubation of EGFP(Δ17)hM1 cells with increasing concentrations of brucine (Fig. 3A) led to a dose-dependent slowing down of Bo(12)Pz association (k_{app} values for the fast binding step vary from 0.034, 0.016 to 0.0096 sec^{-1} in the absence and the presence of 100 or 500 µM brucine, respectively). Interestingly, brucine slightly increased the amplitude of EGFP fluorescence extinction at Bo(12)Pz binding equilibrium. Such a small potentiation might be related to the use of an almost saturating tracer concentration (200 nM). Brucine modulated Bo(10)Pz binding very similarly whereas gallamine reduced both the association rate and the amplitude of Bo(10)Pz and Bo(12)Pz binding at equilibrium (not shown).

As shown in Fig. 3B, and in agreement with previous findings on Bo(10)Pz binding properties (Tahtaoui et al., 2004), brucine (in the presence of a saturating concentration of atropine) induced a profound deceleration of Bo(12)Pz dissociation. Brucine alone (up to 2.5 mM) did not promote any dissociation of ligand-receptor complexes (not shown). Brucine had a greater impact on dissociation than on association kinetics (at 100 µM, on- and off- rates were reduced by 2- and 5- fold, respectively), another indication in favour of a positive modulation of Bo(12)Pz affinity. Bo(10)Pz and Bo(12)Pz dissociation from EGFP(Δ17)hM1 receptors were dose-dependently retarded by brucine (Fig. 3C) and by gallamine (Fig. 3D), with half-maximal effects defining the $EC_{50,diss}$ values reported in Table 1.

Molecular Pharmacology Fast Forward. Published on April 19, 2013 as DOI: 10.1124/mol.113.085670
This article has not been copyedited and formatted. The final version may differ from this version.

Identical experimental conditions were applied to the second series of fluorescent derivatives. Bo(15)Pz association rate (k_{app} values for the fast binding step are 0.040, 0.011 or 0.004 sec^{-1} in the absence and the presence of 100 or 500 μM brucine, respectively) and binding amplitude at equilibrium (Fig. 3E) were both reduced by brucine, indicating either a competitive or a negatively cooperative mode of interaction. The first hypothesis was privileged as the dissociation of Bo(15)Pz-receptor complexes (Fig. 3F), and Bo(22)Pz ones (not shown), followed superimposable kinetics when using saturating concentrations of atropine or brucine, alone or in combination, to prevent tracer re-association.

Control Bo(10)Pz and Bo(22)Pz off-rate constants (sec^{-1} x 10^{-4}; mean values for two separate determinations) did not significantly vary whether determined using the classical 'isotopic' (Bo(10)Pz : 6 ± 1; Bo(22)Pz : 14 ± 1) or the 'volumetric' (Bo(10)Pz : 5 ± 1; Bo(22)Pz : 13 ± 1; plus or minus atropine) dilution protocol. Finally, the possibility for BoPz tracers to recruit the indocarbazolole 'WIN' allosteric site (Lazareno et al., 2000, 2002) was ruled out as staurosporine (10 μM) and Win 51,708 (100 μM) slowed down, though to various extents, Bo(10,12)Pz and Bo(15,22)Pz dissociation rates (not shown).

FRET studies : Equilibrium binding properties of BoPz derivatives.

To further explore the origin of their distinct behaviour, BoPz ligands were examined for their equilibrium binding properties under FRET conditions. EGFP(Δ17)hM1 cells were incubated with the fluorescent tracers in physiological buffer, at 20°C to minimize receptor and ligand internalization, and for 22 h to ensure equilibrium even in the presence of allosteric ligands (Lazareno and Birdsall 1995). Saturation studies provided very similar equilibrium dissociation constants for all tracers (Table 1), as previously reported (Tahtaoui et al., 2004).

Competition-type experiments were undertaken using typical orthosteric (atropine and pirenzepine) and allosteric (gallamine and brucine) muscarinic receptor ligands (Fig. 4A).

Molecular Pharmacology Fast Forward. Published on April 19, 2013 as DOI: 10.1124/mol.113.085670
This article has not been copyedited and formatted. The final version may differ from this version.

Atropine and pirenzepine fully displaced Bo(12)Pz binding according to a competitive mode of interaction at the orthosteric receptor site. Submaximal inhibition by gallamine was consistent with saturable negative binding cooperativity. Brucine clearly potentiated Bo(12)Pz binding (taken here at a concentration below its K_d value). Analyses according to the allosteric ternary complex model (Ehlert 1988) yielded estimates of their equilibrium dissociation constant K_x for free EGFP(Δ17)hM1 receptors and of the cooperativity factor α as a measure of their impact on Bo(12)Pz affinity (Table 1).

When using Bo(15)Pz as the tracer (Fig. 4B), all compounds, including brucine and gallamine, displayed a competitive-like binding behaviour. Bo(22)Pz, again, shared Bo(15)Pz properties. Figure 4c illustrates Bo(22)Pz saturation experiments performed in the absence or the presence of brucine (50, 200 and 500 µM). Brucine promoted a homogenous dextral shift of occupancy curves, with a decrease in Bo(22)Pz apparent affinity (K_{app} values) which was submitted to Lew and Angus analysis (Fig. 4B insert). With a 'Schild' slope factor not significantly different from 1 (1.03 ± 0.04), the hypothesis for a competitive interplay between brucine and Bo(22)Pz binding was clearly privileged. Moreover, the affinity constant for brucine (40.7 ± 2.9 µM) determined here was comparable to that (44.9 ± 6.1 µM) defined from similar saturation experiments performed with Bo(15)Pz and in overall agreement with K_x and K_i values derived from competition experiments (Table 1).

Table 1 summarizes drug binding parameters at EGFP(Δ17)hM1 receptors as afforded from FRET experiments using each of the four fluorescent pirenzepine derivatives as an individual tracer. As expected, drug affinity constants at the free receptor do not significantly vary with tracer type or underlying binding mechanism. They are in overall agreement with affinity values reported in the literature ([^{3}H]-NMS binding, M1-enriched membrane preparations) for atropine and pirenzepine (Caulfield and Birdsall 1998), gallamine (Matsui et al. 1995; Lazareno et al., 2000; Fruchart-Gaillard et al., 2006) and brucine (Gharagozloo et al.

Molecular Pharmacology Fast Forward. Published on April 19, 2013 as DOI: 10.1124/mol.113.085670
This article has not been copyedited and formatted. The final version may differ from this version.

1999; Fruchart-Gaillard et al., 2006). The equivalence of $EC_{50,diss}$ and $\alpha.K_x$ parameters for gallamine and brucine suggests that variations in their affinity for free and Bo(10,12)Pz-occupied receptors are driven by binding cooperativity within a ternary allosteric complex. Thus, kinetic and equilibrium FRET studies provided a robust information on BoPz binding properties at M1 receptors, with a clear-cut distinction between Bo(10,12)Pz and Bo(15,22)Pz series of ligands regarding the recruitment of the 'gallamine' allosteric site.

An orthosteric [^{3}H]-NMS point of view on BoPz binding properties.

A series of experiments was done using EGFP(Δ17)hM1 cells, [^{3}H]-NMS as the radioactive orthosteric tracer and unchanged incubation conditions (physiological buffer, 22 h incubation time at 20°C to ensure equilibrium). Displacement experiments were performed at two [^{3}H]-NMS concentrations (ca. $1\times K_d$ and $10\times K_d$) in order to better distinguish competitive from negatively cooperative modes of interaction (Birdsall and Lazareno, 2005; May et al., 2007). Slope factors for all inhibition curves did not statistically differ from 1.

As shown in Fig. 5A, atropine fully displaced specific [^{3}H]NMS binding at low and high tracer concentrations, as expected for competition at the orthosteric receptor site. Gallamine displayed a typical submaximal inhibition (with plateau levels depending on [^{3}H]NMS concentration) consistent with negative binding cooperativity. Brucine was a very partial displacer, featuring almost neutral binding cooperativity with [^{3}H]NMS. Analyses according to the allosteric ternary complex model yielded affinity (K_x) and cooperativity factor (α) estimates (Table 2) in agreement with literature reports for gallamine (Matsui et al., 1995; Lazareno et al., 2000; Fruchart-Gaillard et al., 2006) and brucine (Gharagozloo et al., 1999; Fruchart-Gaillard et al., 2006).

Bo(10)Pz and Bo(15)Pz displayed an apparent competitive mode of interaction (Fig. 5B) as did the two other derivatives. Their K_i values listed in Table 2 closely match K_d values determined under FRET conditions (Table 1). An interesting information (Fig. 5B) was

Molecular Pharmacology Fast Forward. Published on April 19, 2013 as DOI: 10.1124/mol.113.085670
This article has not been copyedited and formatted. The final version may differ from this version.

provided by the Bo(5) compound which lacks the pirenzepine moiety (Fig. 1) and exhibits negative binding cooperativity with [^{3}H]NMS in the low micromolar range. Thus, the Bodipy fluorophore may be able per se to interact with an M1 allosteric site.

This prompted us to test Bo(5), Bo(10)Pz and Bo(15)Pz derivatives (in the presence of 10 µM atropine to prevent [^{3}H]-NMS reassociation) for their ability to alter [^{3}H]NMS off-rate from EGFP(Δ17)hM1 receptors (Fig. 5C). All kinetics followed a monoexponential time course. As expected for a competitive interplay at the orthosteric site, the addition of atropine or pirenzepine (alone or in combination) led to superimposable dissociation traces (control k_{off} = 0.043 ± 0.001 min^{-1}; n = 6). Gallamine and brucine, taken here as references at 200 µM, strongly impacted [^{3}H]NMS dissociation rate. Bo(5) and Bo(10,15)Pz compounds, at 10 µM (i.e. 25- and 1000-fold their respective equilibrium affinity constants), significantly retarded [^{3}H]NMS dissociation. The possibility for Bo(10)Pz to bind to [^{3}H]-NMS-occupied receptors was totally unexpected as previous FRET (Table 1) and equilibrium [^{3}H]-NMS (Table 2) studies privileged a conventional orthosteric nature for this derivative.

Figure 5D depicts the concentration-dependence of the retardation effects of the allosteric modulators gallamine and brucine and of the three fluorescent derivatives on [^{3}H]-NMS dissociation from EGFP(Δ17)hM1 receptors. In agreement with M1 literature, brucine (Gharagozloo et al., 1999) and gallamine (Matsui et al., 1995) fully inhibited [^{3}H]-NMS dissociation with $EC_{50,diss}$ values close to 30 and 110 µM, respectively, reflecting their affinity for [^{3}H]-NMS-occupied receptors (Table 2). Fluorescent derivatives could not be tested at concentrations above 30 µM because of stock and solubility limitations. Nevertheless, their retardation effect on [^{3}H]-NMS dissociation manifested a net concentration-dependency. Bo(10)Pz and Bo(15)Pz curves were almost superimposable and Bo(15)Pz effect ($EC_{50,diss}$ 3.5 ± 0.4 µM, n=3) was probably partial ($E_{max,diss}$ 72.5 ± 2.5 %, n=3).

Molecular Pharmacology Fast Forward. Published on April 19, 2013 as DOI: 10.1124/mol.113.085670
This article has not been copyedited and formatted. The final version may differ from this version.

Rationale behind the selection of M1 W400 and W405 receptor mutants.

Accumulating evidence supports the bitopic character of the BoPz derivatives : they recognize epitopes within both orthosteric (competitive character when tested against orthosteric ligands in functional and equilibrium binding assays) and allosteric (retardation of [^{3}H]-NMS dissociation) sites. There is no doubt that the Bo(15,22)Pz compounds may bridge the orthosteric and the 'gallamine' sites (kinetic and equilibrium FRET experiments) but the nature and the position of the allosteric domain recruited by Bo(10,12)Pz are still unclear.

To address this question, we considered an ensemble of observations pointing the M1 W400 and W405 residues as interesting mutagenesis probes : a) the Bodipy fluorophore may bind to an allosteric site (Bo(5) data; Fig. 5B), b) the aromatic Bodipy moiety is well-suited to elicit a π-π stacking with the indole ring of a Trp residue, c) the EGFP (donor)-Bodipy (acceptor) distances for the Bo(10,12)Pz and Bo(15,22)Pz subgroups, as determined from FRET efficacy (Tahtaoui et al., 2004), only differ by 3-5 Å, d) the conserved Trp400 (7.35) and Trp405 (7.40) residues (numbering according to Ballesteros-Weinstein convention, 1995 indicated under parentheses) are spatially close, one α-helical turn apart on top of TM7, and most importantly e) the conserved Trp at position 7.35 is regarded as a key component of the prototypical 'gallamine' allosteric site of mAChRs (Matsui et al. 1995; Prilla et al., 2006).

Impact of mutations on orthosteric and allosteric ligand binding properties

The properties of the EGFP(Δ17)hM1 receptor, with its Trp400 or Trp405 residues replaced by Ala or Phe (to preserve the aromatic character), were examined through [^{3}H]-NMS binding experiments. Results are shown in Figure 6A and summarized in Table 3.

[^{3}H]-NMS saturation studies indicated a modest impact of the mutations on receptor expression levels, with maximal 2-fold variations in B_{max} values (W405F, increase; W400A, decrease) as compared to wild-type. High [^{3}H]-NMS affinity was preserved, as reported for

Molecular Pharmacology Fast Forward. Published on April 19, 2013 as DOI: 10.1124/mol.113.085670
This article has not been copyedited and formatted. The final version may differ from this version.

the M1 W400 mutant (Matsui et al., 1995) and for homologous W400 (^{M2}W422, ^{M5}W477) and W405 (^{M2}W427, ^{M5}W482) mutations in M2 and M5 receptors (Prilla et al., 2006).

Competition studies pointed to an unchanged atropine affinity, a discrete alteration in pirenzepine affinity related to the suppression of the aromatic nature of the residues (as shown for the M1 W400 mutant; Matsui et al., 1995) and an increase in carbachol affinity for the EGFP-W405 construct. An elevation in agonist affinity and constitutive activity has been already noticed for this M1 mutant (Matsui et al., 1995; Lu et al., 2001) and interpreted as a consequence of the destabilization of a ground-state intramolecular contact network..

[^{3}H]-NMS equilibrium and kinetic studies pointed to a 2-fold reduction in gallamine affinity at free EGFP-W405A/F receptors and to a slight reduction in its binding cooperativity with NMS. In contrast, the W400A/F mutations led to a more than 10-fold decrease in gallamine affinity at free- and [^{3}H]-NMS-occupied receptors, with little impact on binding cooperativity. These data are in agreement with previous reports on gallamine properties at the W400A/F M1 mutants (Matsui et al., 1995) and at the alanine mutants of the homologous W400 and W405 residues in M2 and M5 receptors (Prilla et al., 2006). Alterations in brucine modulation were more difficult to ascertain given its neutral cooperativity with [^{3}H]-NMS binding. The impact of the two series of mutations was thus best apprehended from dissociation kinetics which again pointed to the crucial importance of the W400 residue. At variance with gallamine, the affinity of brucine ($EC_{50,diss}$ value) for [^{3}H]-NMS-occupied EGFP-W405A/F receptors was slightly but significantly increased, as compared to wild-type. All these controls confirm that the fusion of EGFP to a hM1 receptor with a truncated N-terminus does not modify mutation binding phenotypes and extend available information on the role of the W405 residue in M1 orthosteric and allosteric ligand binding.

Molecular Pharmacology Fast Forward. Published on April 19, 2013 as DOI: 10.1124/mol.113.085670
This article has not been copyedited and formatted. The final version may differ from this version.

Differential alterations of BoPz binding properties at W400 and W405 M1 mutants.

The binding affinity profiles of BoPz ligands at EGFP-W400A/F and EGFP-W405A/F receptor mutants were examined through competition (taking [^{3}H]-NMS as the tracer) and FRET saturation (taking each BoPz derivative as a fluorescent tracer) studies. As shown in Table 4, K_i and K_d values are in remarkable agreement with the exception of Bo(12)Pz and Bo(15)Pz affinities at the EGFP-W400F mutant that differ by a factor of 2 to 3. Another general observation is that substitution of Trp for Phe is less well tolerated than Ala insertion (Bo(15)Pz and Bo(22)Pz binding at the W400 mutants are noticeable exceptions).

Figure 6B illustrates the impact of mutations on equilibrium binding properties of the fluorescent derivatives. Bo(10,12)Pz compounds displayed a similar and moderate sensitivity to the mutation of the W405 residue but did not discriminate between EGFP-400A/F mutants and wild-type receptors, at variance with the prominent role of the W400 residue in Bo(15,22)Pz binding. Bo(15)Pz was actually severely impacted by all mutations (with a 10-fold decrease in affinity at the W405F and W400A mutants). Bo(22)Pz displayed an intermediate profile, with a weaker contribution of the W405 residue (especially when replaced by Ala). Altogether, these findings provide additional support to the delineation of two subgroups of BoPz ligands with differential sensitivity to W405 (10-12 series) or W400 (15-22 series) mutations. They also reinforce the idea that their Bodipy moiety, depending on linker length, may explore distinct (or partially overlapping) allosteric epitopes, including (15-22 series) or not (10-12 series) the key W400 ‘gallamine’ residue.

To get deeper insight into the role of the two tryptophan residues, kinetic studies were carried out to compare [^{3}H]-NMS and BoPz dissociation rates at the four mutants (Table 5). [^{3}H]-NMS dissociation was slightly retarded in all mutants, with a more significant impact of the W405 substitution. These findings corroborate previous reports on [^{3}H]-NMS dissociation from M1 W400A/F (Matsui et al., 1995) and M2 homologous W400A and W405A (Prilla et

Molecular Pharmacology Fast Forward. Published on April 19, 2013 as DOI: 10.1124/mol.113.085670
This article has not been copyedited and formatted. The final version may differ from this version.

al., 2006) mutants. As none of these mutations have relevant effects on [^{3}H]-NMS affinity, association and dissociation steps are probably retarded to the same extent. Thus, Trp405, and to a minor degree Trp400, may have a structural role in maintaining proper access of [^{3}H]-NMS to- and egress from- the M1 orthosteric pocket.

In contrast with [^{3}H]-NMS, the dissociation of BoPz tracers was accelerated in all instances, most often very similarly at Ala and Phe mutants (Table 5). Bo(15)Pz and Bo(22)Pz took some benefit from an aromatic Phe residue to compensate for kinetic alterations. Obviously, increases in off-rates of Bo(10)Pz from W405F and W400A/F receptors, and of all other derivatives from all mutants, account for the decreases in affinity observed under equilibrium conditions (Table 4). More attention was paid to Bo(10)Pz dissociation from the W405A mutant as, in marked contrast with all other BoPz derivatives, it proceeded according to a biphasic process. An empirical two-exponential model was adopted to fit its dissociation traces : a fast (k_{off} : 0.19 ± 0.01 sec^{-1}) and a slow (k_{off} : 0.0065 ± 0.0001 sec^{-1}) component, contributing by 40 and 60 % respectively to Bo(10)Pz binding reversal amplitude, best described its dissociation when promoted by 10 µM atropine. Gallamine and brucine revealed striking differences in their ability to modulate rates and relative amplitudes of both phases (preliminary observation). Underlying mechanisms merit further investigation.

We finally investigated through FRET the impact of the four point mutations on gallamine and brucine affinity parameters at free (equilibrium studies) and BoPz-occupied (dissociation studies) receptors (Supplemental Table S1). This allowed us to verify that the determination of gallamine affinity for each free receptor mutant is rather robust : affinity constants are independent of the nature of the BoPz tracer and similar to those afforded from [^{3}H]-NMS equilibrium studies (Table 3). The same observation applied to brucine, although the comparison was limited by the neutral cooperativity behaviour it manifested in many instances : for example, its weakly positive cooperativity with Bo(10,12)Pz binding on the

Molecular Pharmacology Fast Forward. Published on April 19, 2013 as DOI: 10.1124/mol.113.085670
This article has not been copyedited and formatted. The final version may differ from this version.

wild-type receptor shifted to neutral cooperativity on the W400A/F mutants. Bo(10,12)Pz equilibrium studies also revealed a stronger negative binding cooperativity with gallamine on the W400F mutant. An important point, based on equilibrium and kinetic data from all mutants, is that gallamine and brucine preserved their competitive character with Bo(15,22)Pz binding we illustrated several ways on the wild-type EGFP(Δ17)hM1 receptor. Last, it is worth mentioning the pronounced loss of efficacy of gallamine to inhibit Bo(10,12)Pz dissociation from W400A/F mutants, reflected in an up to 30-fold increase in its $EC_{50,diss}$ value and in a reduction in maximal retardation effect (especially at the W400A mutant).

Validation of an M1 receptor homology model and ligand docking

The recent resolution of the crystal structures of the human M2 (Haga et al., 2012) and rat M3 (Kruse et al., 2012) muscarinic receptors, both in an inactive state and in complex with non selective antagonists, revealed their great similarity. Structural conservation includes the organization of their transmembrane domains (7TM), an identical fold of their extracellular loops (despite a low sequence conservation) and a deeply buried orthosteric binding pocket (delimited by residues absolutely conserved among the five mAChRs) separated from a solvent accessible vestibule by a narrow gate surrounded by three conserved tyrosine (Tyr3.34, Tyr6.51 and Tyr7.39) residues. On the basis of these observations and of overall sequence conservation (49.7% sequence identity between M1 and M3; 45.0% between M1 and M2), the M3 receptor was selected as the template to model M1 structure.

3-quinuclidinyl benzilate (QNB) and tiotropium bind in a remarkable similar pose to M2 and M3 receptors (Kruse et al., 2012) that is likely to represent a conserved binding mode for structurally close anticholinergics. We were therefore interested to examine whether this could also apply to pirenzepine binding in our M1 model (Supplemental Fig. S2). This was indeed the case as all three antagonists are enclosed in a highly conserved aromatic cage, establish an ionic bond with Asp3.33 and fit a common 3D pharmacophore defined by a

Molecular Pharmacology Fast Forward. Published on April 19, 2013 as DOI: 10.1124/mol.113.085670
This article has not been copyedited and formatted. The final version may differ from this version.

positively charged nitrogen atom in an aliphatic 6-membered ring, a carbonyl group, and two aromatic rings. This allowed us to build the M1-pirenzepine complex, to show (Fig. 7A) that pirenzepine binding pose well mimicks that of the two other antagonists in M2 and M3 crystal structures, and to validate our M1 model, at least from the orthosteric site point of view.

A more global image of the M1 receptor model is provided in Figure 7B. It allows to see that the cavity in the 7TM M1 receptor core displays a highly hydrophobic region at the junction between the orthosteric site and the allosteric vestibule, in the vicinity of the side chain of Trp101 in TM3. The two residues which were mutated in this study, Trp400 and Trp405, sit respectively in the vestibule and at the TM7/lipid bilayer interface. They form the ends of a network of aromatic residues bridging TM helices (including the Tyr106-Tyr381-Tyr404 triad but also Tyr82, Tyr85, Trp91, Trp101, Trp157 and Tyr408) and may lock its conformation. This M1 model provides the structural foundations for further discussion of our experimental data on fluorescent pirenzepine derivatives.

Molecular Pharmacology Fast Forward. Published on April 19, 2013 as DOI: 10.1124/mol.113.085670
This article has not been copyedited and formatted. The final version may differ from this version.

DISCUSSION

We investigated into much detail the binding properties of a series of fluorescent Bodipy-Pirenzepine derivatives at EGFP-fused M1 receptors. A combination of radioligand and FRET binding experiments and of mutagenesis and molecular modeling studies was necessary to demonstrate their bitopic nature : they bind, through their pirenzepine pharmacophore, to the orthosteric site and simultaneously occupy, through their Bodipy moiety, the M1 allosteric vestibule (Fig. 7). While long (15-22 atoms) linkers allow the fluorophore to access to the gallamine/brucine site, shorter (10-12 atoms) linkers confine it within a neighbouring but separate allosteric subdomain.

Pirenzepine and BoPz compounds display similar affinities (10 nM range), suggesting a weak contribution of the fluorophore to overall binding energy of the derivatives. Such a view is supported by the observation of monophasic and unchanged dissociation kinetics for all BoPz derivatives, whatever the protocol which is applied. Thus, the fluorescent ligands display an homogenous binding mode and probably firmly anchor to the receptor through binding of their pirenzepine moiety within the orthosteric site. One should mention, however, that the Bo(5) fragment has allosteric affinity in the low micromolar range and that Bo(15,22)Pz binding is clearly impacted by W400A/F mutations while that of pirenzepine is much less affected. These latter findings suggest that both the linker and the pirenzepine pharmacophore help the Bodipy moiety to reach a local concentration high enough to interact with allosteric residues.

When examined from the orthosteric point of view, all BoPz derivatives exhibit either competitive-like (when tested against [^{3}H]-NMS and other orthosteric compounds under equilibrium conditions) or allosteric (as afforded from their ability to alter [^{3}H]-NMS dissociation kinetics) properties. Such a mixed orthosteric/allosteric behaviour is often observed for bitopic ligands (Mohr et al, 2010; Valant et al., 2012; Daval et al., 2012). Other

Molecular Pharmacology Fast Forward. Published on April 19, 2013 as DOI: 10.1124/mol.113.085670
This article has not been copyedited and formatted. The final version may differ from this version.

explanations include a strong negative binding cooperativity with [^{3}H]-NMS (if one considers BoPz affinity ratios at free and [^{3}H]-NMS-occupied receptors) or a differential positioning of these derivatives, depending on orthosteric site occupancy. Although retardation of [^{3}H]-NMS dissociation occurs at high BoPz concentrations, fluorophore-driven occlusion and occupancy of the allosteric vestibule by the bulky BoPz derivatives are unlikely. An alternate possibility is to consider an interaction of their pirenzepine moiety with a peripheral site that sterically hinders [^{3}H]-NMS egress from the orthosteric pocket. Indeed, real time FRET monitoring of Bo(10)Pz binding kinetics at EGFP-fused M1 receptors indicated that an initial fast and low affinity binding event, occuring at the receptor surface close to EGFP, precedes ligand translocation within the transmembrane core (Ilien et al, 2009). Molecular dynamic simulations of tiotropium binding to M2 and M3 receptors also revealed the possibility for an orthosteric ligand to pause within the allosteric vestibule while entering or dissociating from the orthosteric pocket (Kruse et al, 2012).

FRET experiments provided further information on BoPz properties, now regarded as individual tracers. Indeed, equilibrium and kinetic FRET data indicated that i) all BoPz derivatives involve an orthosteric binding component, ii) Bo(10,12)Pz affinity is allosterically modulated by brucine (potentiation) and gallamine (inhibition); thus, their capacity to alter [^{3}H]-NMS dissociation rate probably originates from the recruitment of allosteric epitopes that do not overlap with the classical allosteric domain, iii) Bo(15,22)Pz, in marked contrast with the former ligands, inherit allosteric properties from occupancy of the gallamine/brucine site and iv) Bo(15,22)Pz dissociation proceeds similarly whatever the agent (atropine, brucine or gallamine) selected to prevent tracer re-association to the receptor, as expected for concomitant binding of pirenzepine and Bodipy moieties according to a bitopic pose.

Mutagenesis experiments, focused on the impact of W400A/F and W405A/F point mutations on orthosteric, allosteric and BoPz ligand binding properties, provided additional

Molecular Pharmacology Fast Forward. Published on April 19, 2013 as DOI: 10.1124/mol.113.085670
This article has not been copyedited and formatted. The final version may differ from this version.

support to the idea that the Bodipy moiety in Bo(10,12)Pz and Bo(15,22)Pz derivatives reach distinct allosteric binding epitopes. Indeed, Bo(10,12)Pz binding is slightly, but significantly, altered by mutations of the W405 residue whereas Bo(15,22)Pz, gallamine and brucine display marked losses in affinity at the W400A/F mutants. However, Bo(15)Pz and to a lesser extent Bo(22)Pz show also a significant reduction in affinity upon Ala/Phe substitution of the W405 residue. Thus, a preferential location of their fluorophore within the gallamine site does not exclude the possibility for it, provided the linker is long enough, to explore neighbouring domains within the allosteric vestibule (Fig. 7). Keeping in mind that mutagenesis data do not prove a direct implication of these Trp residues, one cannot exclude the destabilization of the aromatic network to which they belong to be responsible for alterations in global positioning of BoPz derivatives within the receptor (Hulme et al., 2007; our modeling studies). Indeed, variations in off-rates for [^{3}H]-NMS (slower) and fluorescent tracers (faster) from the four M1 mutants may result from a partial collapse of the allosteric lid, hindering [^{3}H]-NMS to egress from the orthosteric domain or the fluorophore of BoPz ligands to properly anchor to an allosteric site.

These data highlight the prominent role of linker length in the definition of the bitopic nature and the selection of different allosteric binding poses for BoPz compounds. Previous reports already indicated that the fusion of bulky groups (including fluorophores) to pirenzepine was well tolerated in terms of affinity provided the linker was long enough (at least 6 to 10 methylenes) to relax the constraints imposed by pirenzepine binding to the M1 orthosteric site (Karton et al, 1991; Tahtaoui et al, 2004). Although the nature (PEG or isopeptidic) of the linker seems here of marginal importance, the examples of Bo(5) and of similar derivatives (Daval et al., 2012) clearly indicate that the linker conveys affinity and negative binding cooperativity to these molecules.

Molecular Pharmacology Fast Forward. Published on April 19, 2013 as DOI: 10.1124/mol.113.085670
This article has not been copyedited and formatted. The final version may differ from this version.

Valuable insights into linker-guided positioning of the fluorophore of Bo(10,12)Pz and Bo(15,22)Pz compounds were gained from M1 modeling and ligand docking studies. The structures of all ligand-receptor complexes were built assuming a fixed pose for pirenzepine (substituted or not) we found to perfectly fit a 3D-pharmacophore (Fig. 7A) common to QNB and tiotropium in M2 and M3 (Kruse et al., 2012) receptors, respectively. Interestingly, the distal N-methyl group of pirenzepine (the anchor point for the linker) is not oriented towards the larger opening between the orthosteric and allosteric modules (Fig. 7B). Instead, it faces a narrow channel (between Asp105, Tyr404 and Tyr408 residues), filled with a water molecule in the M2 structure (Haga et al., 2012). In BoPz-M1 complexes (Fig. 7C, D), the linker passes through this channel, hence replacing the water molecule, to reach the most hydrophobic region of the cavity (Fig. 7B; brown shaded area), nearby Trp101. This configuration fixes the position of the first seven atoms of the linker (close to pirenzepine), thereby restricting possibilities for positioning the fluorophore, especially if the linker is short. Experimental support to this view is provided by the measurement of a 10-fold faster off-rate of the Bo(10)Pz compound from the W101A M1 mutant (unpublished data). In Bo(10)Pz-M1 complexes (Fig. 7C), the Bodipy group locates at the entrance of the vestibule, in an opening between TM2 and TM7, yet in a position compatible with concomitant binding of brucine or of gallamine. When presented as volumes, these allosteric modulators best evidence plugs over the orthosteric pocket (Supplemental Fig. S3). Long linkers, such as in Bo(22)Pz (Fig. 7D), fold into the allosteric cavity nearby Trp400 and allow the fluorophore to locate between ecl2 and ecl3, so that the binding of brucine and gallamine is prevented.

These models nicely account for most our experimental observations, including the estimation of a distance (10 Å) between the Bodipy boron atoms in Bo(10)Pz- and Bo(22)Pz-receptor complexes which rather well coincides with average difference in EGFP-Bodipy separation (5 Å) determined from FRET efficacy using the same derivatives (Tahtaoui et al., 2004). One

Molecular Pharmacology Fast Forward. Published on April 19, 2013 as DOI: 10.1124/mol.113.085670
This article has not been copyedited and formatted. The final version may differ from this version.

should add here that docking solutions are consistent with multiple placement of the fluorophore within a large and well-accessible receptor vestibule that does not define an enclosed “lock” suitable for tight binding of Bodipy viewed as a “key”. As the fluorophore, according to linker length, is allowed to explore topographically distinct and non conserved allosteric domains, including extracellular loops, it would be interesting to test BoPz ligands for their binding selectivity at M1-M5 receptor subtypes.

In conclusion, this work describes a step-by-step strategy to define the bitopic binding properties of a family of fluorescent pirenzepine derivatives at muscarinic M1 receptors. It highlights the pivotal role of the linker which connects orthosteric and allosteric building blocks within a bitopic ligand. Indeed, it imposes structural constraints to and dictates pharmacological outcomes for the hybrid molecule (including biased signaling as evidenced recently for dualsteric agonists on M2 receptors; Bock et al., 2012) that are not readily predictable from the properties of unconnected partners. Our findings also demonstrate that a fluorophore fused to an orthosteric compound is not an innocent bystander as it may confer an allosteric texture to the resultant tracer. Unless carefully controlled, this may lead to data misinterpretation, especially when working with bioamine receptors which contain vicinal orthosteric and allosteric modules. Thus, the rational design and in-depth study of bitopic molecules may provide, in addition to advantages expected from the combination of orthosteric and allosteric moieties within a single molecule, valuable guidelines to decipher ‘hidden’ dual drug binding properties.

Molecular Pharmacology Fast Forward. Published on April 19, 2013 as DOI: 10.1124/mol.113.085670
This article has not been copyedited and formatted. The final version may differ from this version.

ACKNOWLEDGMENTS

We thank Stéphanie Riché for technical assistance and Patrick Wehrung for HRMS and HPLC analyses.

AUTHORSHIP CONTRIBUTIONS

Participated in research design: Daval, Galzi and Ilien

Conducted experiments: Daval, Kellenberger, Bonnet, Utard and Ilien

Contributed new reagents or analytic tools: Bonnet

Performed data analysis: Daval, Kellenberger and Ilien

Wrote or contributed to writing of the manuscript: Kellenberger, Galzi and Ilien

REFERENCES

Antony J, Kellershohn K, Mohr-Andrä M, Kebig A, Prilla S, Muth M, Heller E, Disingrini T, Dallanoce C, Bertoni S, Schrobang J, Tränkle C, Kostenis E, Christopoulos A, Höltje HD, Barocelli E, De Amici M, Holzgrabe U, and Mohr K (2009) Dualsteric GPCR targeting: a novel route to binding and signaling pathway selectivity. *FASEB J* **23:** 442-450.

Arunlakshana O and Schild HO (1959) Some quantitative uses of drug antagonists. *Br J Pharmacol Chemother* **14:** 47–58.

Avlani VA, Langmead CJ, Guida E, Wood MD, Tehan BG, Herdon HJ, Watson JM, Sexton PM, and Christopoulos A (2010) Orthosteric and allosteric modes of interaction of novel selective agonists of the M1 muscarinic acetylcholine receptor. *Mol Pharmacol* **78:**94-104.

Ballesteros JA and Weinstein H (1995) Integrated methods for the construction of three dimensional models and computational probing of structure-function relationships in G-protein coupled receptors. *Methods Neurosci **25*:** 366-428.

Birdsall NJM, Farries T, Gharagozloo P, Kobayashi S, Lazareno S, and Sugimoto M (1999) Subtype-selective positive cooperative interactions between brucine analogs and acetylcholine at muscarinic receptors : Functional studies. *Mol Pharmacol* **55:** 778-786.

Birdsall NJM and Lazareno S (2005) Allosterism at muscarinic receptors: Ligands and mechanisms. *Mini-Rev Med Chem* **5:** 523-543.

Bock A, Merten N, Schrage R, Dallanoce C, Bätz J, Klöckner J, Schmitz J, Matera C, Simon K, Kebig A, Peters L, Müller A, Schrobang-Ley J, Tränkle C, Hoffmann C, De Amici M, Holzgrabe U, Kostenis E, and Mohr K (2012) The allosteric vestibule of a seven transmembrane helical receptor controls G-protein coupling. *Nature Comm*. **3:** 1-11

Canals M, Lane JR, Wen A, Scammels PJ, Sexton PM, and Christopoulos A (2012) A Monod-Wyman-Changeux mechanism can explain G protein-coupled receptor (GPCR) allosteric modulation. *J Biol Chem* **287**: 650-659.

Caulfield MP (1993) Muscarinic receptors: Characterization, coupling and function. Pharmacol Ther **58:** 319-379.

Christopoulos A, Parsons AM, Lew MJ, and El-Fakahany EE (1999) The assessment of antagonist potency under conditions of transient response kinetics. *Eur J Pharmacol* **382:** 217-227

Conn PJ, Jones CK, and Lindsley CW (2009) Subtype-selective allosteric modulators of muscarinic receptors for treatment of CNS disorders. *Trends Pharmacol Sci* **30**: 148- 155.

Daval S, Valant C, Bonnet D, Kellenberger E, Hibert M, Galzi J-L, and Ilien B (2012) Fluorescent derivatives of AC-42 to probe bitopic orthosteric/allosteric binding mechanisms on muscarinic M1 receptors. *J Med Chem* **55:** 2125-2143.

De Amici M, Dallanoce C, Holzgrabe U, Tränkle C, and Mohr K (2010) Allosteric ligands for G protein-Coupled Receptors : A novel strategy with attractive therapeutic opportunities. *Med Res Rev* **30:** 463-549.

Deupi X and Kobilka BK (2010) Energy landscapes as a tool to integrate GPCR structure, dynamics, and function. *Physiol* **25:** 293-303.

Digby GJ, Shirey JK, and Conn PJ (2010) Allosteric activators of muscarinic receptors as novel approaches for treatment of CNS disorders. *Mol Biosyst* **6:** 1345-1354.

Disingrini T, Muth M, Dallanoce C, Barocelli E, Bertoni S, Kellershohn K, Mohr K, De Amici M, and Holzgrabe U (2006) Design, synthesis, and action of oxotremorine-related hybrid-type allosteric modulators of muscarinic acetylcholine receptors. *J Med Chem* **49:** 366-372.

Eglen RM (2012) Overview of muscarinic receptor subtypes. *Handb Exp Pharmacol* **208:**3-28.

Ehlert FJ (1988) Estimation of the affinities of allosteric ligands using radioligand binding and pharmacological null methods. *Mol Pharmacol* **35:** 187-194.

Ellis J and Seidenberg M (1999) Competitive and allosteric interactions of 6-chloro-5,10-dihydro-5-[(1-methyl-4-piperidinyl)acetyl]-11H-dibenzo[b,e][1,4]diazepine-11-one

hydrochloride (UH-AH 37) at muscarinic receptors, via distinct epitopes. *Biochem Pharmacol* **57:** 181-186.

Fruchart-Gaillard C, Mourier G, Marquer C, Ménez A, and Servent D (2006) Identification of various allosteric interaction sites on M1 muscarinic receptor using ^{125}I-Met35-Oxidized muscarinic toxin 7. *Mol Pharmacol* **69:** 1641-1651.

Gharagozloo P, Lazareno S, Popham A, and Birdsall NJM (1999) Allosteric interactions of quaternary strychnine and brucine derivatives with muscarinic acetylcholine receptors. *J Med Chem* **42:** 438-45.

Giraldo E, Micheletti R, Montagna E, Giachetti A, Vigano MA, Ladinsky H, and Melchiorre C (1988) Binding and functional characterization of the cardioselective muscarinic antagonist methoctramine. *J Pharmacol Exp Ther* **244**: 1016- 1020.

Gregory KJ, Sexton PM, and Christopoulos A (2007) Allosteric modulation of muscarinic acetylcholine receptors. *Curr Neuropharmacol* **5:** 157-167.

Gregory KJ, Hall NE, Tobin AB, Sexton PM, and Christopoulos A (2010) Identification of orthosteric and allosteric site mutations in M2 muscarinic acetylcholine receptors that contribute to ligand-selective bias. *J Biol Chem* **285:** 7459-7474.

Gregory KJ, Sexton PM, Tobin AB, and Christopoulos A (2012) Stimulus bias provides evidence for conformational constraints in the structure of a G protein-coupled receptor. *J Biol Chem* **287:** 37066-37077.

Haga K, Kruse AC, Asada H, Yurugi-Kobayashi T, Shiroishi M, Zhang C, Weis WI, Okada T, Kobilka BK, Haga, T, and Kobayashi T (2012) Structure of the human M2 muscarinic acetylcholine receptor bound to an antagonist. *Nature* **482:** 547-551.

Heikkilä J, Jansson C, and Akerman KEO (1991) Differential coupling of muscarinic receptors to Ca^{2+} mobilization and cyclic AMP in SH-SY5Y and IMR32 neuroblastoma cells. *Eur J Pharmacol* **208:** 9-15.

Hulme EC, Bee MS, and Goodwin J-A (2007) Phenotypic classification of mutants : a tool for understanding ligand binding and activation of muscarinic receptors. *Biochem Soc Trans* **35:** 742-745.

Ilien B, Franchet C, Bernard P, Morisset S, Weill CO, Bourguignon J-J, Hibert M, and Galzi J-L (2003) Fluorescence resonance energy transfer to probe human M1 muscarinic receptor structure and drug binding properties. *J Neurochem* **85:** 768-778.

Ilien B, Glasser N, Clamme J-P, Didier P, Piemont E, Chinnappan R, Daval SB, Galzi J-L, and Mely Y (2009) Pirenzepine promotes the dimerization of muscarinic M1 receptors through a three-step binding process. *J Biol Chem* **284:** 19533-19543.

Jakubik J, El-Fakahany EE, and Tucek S (2000) Evidence for a tandem two-site model of ligand binding to muscarinic acetylcholine receptors. *J Biol Chem* **275:** 18836-18844.

Jakubik J, Tucek S, and El-Fakahany, EE (2002) Allosteric modulation by persistent binding of xanomeline of the interaction of competitive ligands with the M1 muscarinic acetylcholine receptor. *J Pharm Exp Ther* **3012:** 1033-1041.

Karton Y, Bradbury BJ, Baumgold J, Paek R, and Jacobson KA. (1991) Functionalized congener approach to muscarinic antagonists: Analogues of pirenzepine. *J Med Chem* **34:** 2133-2145.

Kenakin T, Jenkinson S, and Watson C (2006) Determining the potency and molecular mechanism of action of unsurmountable antagonists. *J Pharmacol Exp Ther* **319:** 710-723.

Kenakin T and Miller LJ (2010) Seven transmembrane receptors as shapeshifting proteins: The impact of allosteric modulation and functional selectivity on new drug discovery. *Pharmacol Rev* **62:** 265-304.

Kruse AC, Hu J, Pan AC, Arlow DH, Rosenbaum DM, Rosemond E, Green HF, Liu T, Chae PS, Dror RO, Shaw DE, Weis WI, Wess J, and Kobilka BK (2012) Structure and dynamics of the M3 muscarinic acetylcholine receptor. *Nature* **482:** 552-556.

Lanzafame A, Christopoulos A, Mitchelson F (2001) The allosteric interaction of otenzepad (AF-DX 116) at muscarinic M2 receptors in guinea pig atria. *Eur J Pharmacol* **416:** 235–244.

Lazareno S and Birdsall NJM (1995) Detection, quantitation, and verification of allosteric interactions of agents with labeled and unlabeled ligands at G protein-coupled receptors : interactions of strychnine and acetylcholine at muscarinic receptors. *Mol Pharmacol* **48:**362-378.

Lazareno S, Popham A, and Birdsall NJM (2000) Allosteric interactions of staurosporine and other indolocarbazoles with N-[*methyl*-^{3}H]Scopolamine and acetylcholine at muscarinic receptor subtypes : Identification of a second allosteric site. *Mol Pharmacol* **58:** 194-207.

Lazareno S, Popham A, and Birdsall NJM (2002) Analogs of WIN 62,577 define a second allosteric site on muscarinic receptors. *Mol Pharmacol* **62:** 1492-1505.

Lew MJ and Angus JA (1995) Analysis of competitive agonist-antagonist interactions by nonlinear regression. *Trends Pharmacol Sci* **16:** 328-337.

Lu Z-L, Saldanha, JW, and Hulme EC (2001) Transmembrane domains 4 and 7 of the M1 muscarinic acetylcholine receptor are critical for ligand binding and the receptor activation switch. *J Biol Chem* **276:** 34098-34104.

Marcou G and Rognan D (2007) Optimizing fragment and scaffold docking by use of molecular interaction fingerprints. *J Chem Inf Model* **47:**195-207.

Matsui HS, Lazareno S, and Birdsall NJM (1995) Probing of the location of the allosteric site on m1 muscarinic receptors by site-directed mutagenesis. *Mol Pharmacol* **47:** 88-98.

May LT, Leach K, Sexton PM, and Christopoulos A (2007) Allosteric modulation of G protein-coupled receptors. *Annu Rev Pharmacol Toxicol* **47:** 14.1-14.51.

Mohr K and Tränkle C (1994) Allosteric effects of the alkane-bis-ammonium compound W84 and of tacrine on [^{3}H]Pirenzepine binding at M1-receptors in rat cerebral cortex. *Pharmacol Toxicol* **75:** 391-394.

Mohr K, Tränkle C, Kostenis E, Barocelli E, De Amici M, and Holzgrabe U (2010) Rational design of dualsteric GPCR ligands : quests and promise. *Br J Pharmacol* **159:** 997-1008.

Potter LT, Ferrendelli CA, Hanchett HE, Hollifield MA, and Lorenzi MV (1989) Tetrahydroaminoacridine and other allosteric antagonists of hippocampal M1 muscarine receptors. *Mol Pharmacol* **35:** 652-660.

Prilla S, Schrobang J, Ellis J, Höltje H-D, and Mohr K (2006) Allosteric interactions with muscarinic acetylcholine receptors: Complex role of the conserved tryptophan M_2 ^{422}Trp in a critical cluster of amino acids for baseline affinity, subtype selectivity, and cooperativity. *Mol Pharmacol* **70:** 181-193.

Proska J and Tucek S (1994) Mechanisms of steric and cooperative actions of alcuronium on cardiac muscarinic acetylcholine receptors. *Mol Pharmacol* **45:** 709–717.

Raasch A, Scharfenstein O, Tränkle C, Holzgrabe U, and Mohr K (2002) Elevation of ligand binding to muscarinic M2 acetylcholine receptors by bis(ammonio)alkane-type allosteric modulators. *J Med Chem* **45:** 3809-3812.

Redka DS, Pisterzi LF, and Wells JW (2008) Binding of orthosteric ligands to the allosteric site of the M2 muscarinic cholinergic receptor. *Mol Pharmacol* **74:** 834-843.

Steinfeld T, Mammen M, Smith JAM, Wilson RD, and Jasper JR (2007) A novel multivalent ligand that bridges the allosteric and orthosteric binding sites of the M_2 muscarinic receptor. *Mol Pharmacol* **72:** 291-302.

Tahtaoui C, Parrot I, Klotz P, Guillier F, Galzi J-L, Hibert M, and Ilien B (2004) Fluorescent pirenzepine derivatives as potential bitopic ligands of the human M1 muscarinic receptor. *J Med Chem* **47:** 4300-4315.

Tränkle C, Andresen I, Lambrecht G, and Mohr K (1998) M_2 receptor binding of the selective antagonists AF-DX 384: Possible involvement of the common allosteric site. *Mol Pharmacol* **53:** 304-312.

Valant C, Gregory KJ, Hall NE, Scammels PJ, Lew MJ, Sexton PM, and Christopoulos A (2008) A novel mechanism of G protein-coupled receptor functional selectivity. Muscarinic partial agonist McN-A-343 as a bitopic orthosteric/allosteric ligand. *J Biol Chem* **283:** 29312-29321.

Valant C, Lane JR, Sexton PM, and Christopoulos A (2012) The best of both worlds? Bitopic orthosteric/allosteric ligands of G Protein-Coupled Receptors. *Annu Rev Pharmacol Toxicol* **52:** 153-178.

Molecular Pharmacology Fast Forward. Published on April 19, 2013 as DOI: 10.1124/mol.113.085670
This article has not been copyedited and formatted. The final version may differ from this version.

FOOTNOTES

Funding was provided by the CNRS, INSERM and Université de Strasbourg.

Sandrine Daval was a recipient of a grant from the Association Nationale de la Recherche Technique (Convention CIFRE 564/2005 with Prestwick Chemical).

Present adresses (S.D.) : Quintiles, Parc d'Innovation, 67404 Illkirch (France).

Reprint requests to :

Dr Brigitte ILIEN

Unité Biotechnologie et Signalisation Cellulaire

UMR 7242 CNRS, Université de Strasbourg

Ecole Supérieure de Biotechnologie de Strasbourg

300, boulevard S. Brant - BP 10413 ; 67412 ILLKIRCH Cedex (France)

Email : brigitte.ilien@unistra.fr

Molecular Pharmacology Fast Forward. Published on April 19, 2013 as DOI: 10.1124/mol.113.085670
This article has not been copyedited and formatted. The final version may differ from this version.

FIGURE LEGENDS

Figure 1 : The Bodipy-Pirenzepine (BoPz) family of ligands.

The Bodipy [558/568] fluorophore (Bo) is connected to pirenzepine (Pz) through linkers of varying length (10 to 22 atoms) and nature (isopeptidic or polyethylene glycol type). The Bo(5) compound, a propanamide derivative of Bodipy, lacks the pirenzepine moiety. The structures of gallamine and brucine, two allosteric modulators which have been used throughout this study, are also presented.

Figure 2 : Inhibition by Bo(10)Pz, Bo(15)Pz and pirenzepine of acetylcholine-induced calcium mobilization in EGFP(Δ17)hM1 expressing HEK cells and in IMR 32 cells.

Prior to agonist addition, EGFP(Δ17)hM1 expressing HEK cells (top panel) and IMR 32 cells (lower panel) were pre-incubated for 10 min at 20°C with vehicle (control; open symbol) or with increasing concentrations (in µM) of Bo(10)Pz (● ; 0.03, 0.2, 1), Bo(15)Pz (■ ; 0.05, 0.25, 2) or pirenzepine (◆ ; EGFP(Δ17)hM1 cells : 0.2, 2, 20; IMR 32 cells: 0.03, 0.2, 0.7).

Peak fluorescence intensity values are expressed as a percentage of the control maximal response in each cell line. Data points from typical experiments were submitted to individual curve fitting according to Eq. 1 to derive EC_{50} values and slope factors (non significantly different from 1). Mean EC_{50} ± S.E. values for control dose-responses curves are 94 ± 4 nM (n = 7) and 1.2 ± 0.3 µM (n = 8) for EGFP(Δ17)hM1 and IMR 32 cells, respectively.

Lew-Angus and Schild (insert) plots, shown on the right, were constructed (Eqs. 2 and 3) using sets of EC_{50} values derived from dose-response curves obtained in the absence or presence of Bo(10)Pz (●), Bo(15)Pz (■) or pirenzepine (◆).

Molecular Pharmacology Fast Forward. Published on April 19, 2013 as DOI: 10.1124/mol.113.085670
This article has not been copyedited and formatted. The final version may differ from this version.

Figure 3 : Real-time FRET monitoring of BoPz binding to EGFP(Δ17)hM1 receptors : impact of brucine and gallamine.

Association step (**A**, **E**) : EGFP(Δ17)hM1 cells were pre-incubated for 10 min at 20°C with vehicle (black) or brucine (100 µM: light grey ; 500 µM: dark grey). Following the addition of Bo(12)Pz (**A**) or Bo(15)Pz (**E**) (time 0; 200 nM final concentration), association was monitored over time as a decrease in fluorescence intensity. Amplitudes for fluorescence extinction (in %) at binding equilibrium in control, 100 µM and 500 µM-brucine treated cells were respectively of 36, 40 and 45 (Bo(12)Pz) and of 34, 32 and 27 (Bo(15)Pz).

Dissociation step (**B**, **F**) : Cells were first equilibrated for 20 min at 20°C with 200 nM Bo(12)Pz or Bo(15)Pz. Bo(12)Pz dissociation (**B**) started with the addition (time 0) of 5 µM atropine alone (black) or combined with various concentrations of brucine (3, 10, 30, 100 and 200 µM). Bo(15)Pz dissociation (**F**) proceeded similarly except that it was initiated either with 5 µM atropine alone (black) or combined with 500 µM brucine (light grey), or with 2 mM brucine alone (dark grey). Tracer dissociation was monitored as a recovery in fluorescence intensity over time and expressed as a percentage of the fluorescence extinction amplitude at binding equilibrium. All traces followed a monoexponential decay for fluorescence and dissociation rate constants were derived from fitting to Eq. 7. Off-rate values ($sec^{-1}.10^{-4}$) for Bo(15)Pz ranged from 9 (atropine), 11 (brucine) to 12 (atropine plus brucine).

Dose-dependency for the allosteric delay of Bo(10)Pz (◆) and Bo(12)Pz (□) dissociation (**C**, **D**) : Off-rate constants for the tracers in the presence of modulator ($k_{off,obs}$), relative to control (5.8 and 15.8 $sec^{-1}.10^{-4}$ for Bo(10)Pz and Bo(12)Pz, respectively), were plotted as a function of brucine (**C**) or gallamine (**D**) concentration. Data are means ± S.E. for three independent experiments. Application of Eq. 8 allowed the determination of $EC_{50,diss}$ and $E_{max,diss}$ parameters listed in Table 1.

Molecular Pharmacology Fast Forward. Published on April 19, 2013 as DOI: 10.1124/mol.113.085670
This article has not been copyedited and formatted. The final version may differ from this version.

Figure 4 : Effects of orthosteric and allosteric compounds on equilibrium binding properties of fluorescent tracers to EGFP(Δ17)hM1 receptors.

Competition experiments were performed on EGFP(Δ17)hM1 cells, using either Bo(12)Pz (**A**; 30 nM; 15 nM when tested against brucine) or Bo(15)Pz (**B**; 30 nM; 200 nM when tested against brucine) as the tracer and increasing concentrations of atropine (○), pirenzepine (●), gallamine (◇) or brucine (◆). Specific tracer binding at equilibrium was measured by FRET (Materials and Methods). B/B_0 ratios are means ± S.E. for three independent experiment. Best fits to a competitive (residual binding at high drug concentration non statistically different from 0; Eq. 4) or an allosteric (Eq. 5) model are shown. Parameters are listed in Table 1.

Saturation-type experiments (**C**) were performed using Bo(22)Pz as the fluorescent tracer, in the absence (▲) or the presence of fixed concentrations of brucine (50µM : △; 200µM : ▼ or 500µM : ▽). Specific binding (B) is expressed as a fraction of B_{max}, the maximal FRET amplitude determined at saturating Bo(22)Pz concentrations in the absence of brucine. Mean values ± S.E. for three separate experiments are presented. Individual curve fitting was performed according to Eq.1 (maximal binding levels and slopes constrained to 1) to derive the apparent affinity constants K_{app} for Bo(22)Pz binding. *Inset* : A plot of pK_{app} (-log M) values versus brucine concentration was analysed according to Lew and Angus Eq.3, providing a pK value of 4.39 ± 0.03 and a slope not significantly deviating from 1.

Figure 5 : Impact of unlabelled drugs and fluorescent compounds on equilibrium binding and dissociation kinetics of [^{3}H]-NMS at EGFP(Δ17)hM1 receptors.

A : Competition experiments were performed at low (dashed lines) or high (solid lines) [^{3}H]-NMS concentrations with atropine (○ : 90 or 770 pM [^{3}H]-NMS), gallamine (◇ : 90 or 925 pM [^{3}H]-NMS) or brucine (□ : 140 pM [^{3}H]-NMS). Fractional occupancy B/B_0 values are

Molecular Pharmacology Fast Forward. Published on April 19, 2013 as DOI: 10.1124/mol.113.085670
This article has not been copyedited and formatted. The final version may differ from this version.

means ± S.E. from three independent experiments. Curve fitting is based on Eqs. 4 (atropine) and 5 (gallamine, brucine; K_x parameter for brucine constrained to $EC_{50,diss}$ / α).

B : Competition experiments were performed at low (dashed lines) or high (solid lines) [^{3}H]-NMS concentrations with Bo(10)Pz (● : 52 or 650 pM [^{3}H]-NMS), Bo(15)Pz (▲ : 52 or 735 pM [^{3}H]-NMS) or Bo(5) (■ : 87 pM [^{3}H]-NMS). Data from these typical experiments were fitted according to Eq. 4 (Bo(10)Pz and Bo(15)Pz) or Eq. 5 (Bo(5) derivative).

C : Dissociation of [^{3}H]-NMS from EGFP(Δ17)hM1 receptors was followed at 25°C after addition of 10 µM atropine alone (control; ○) or combined with 10 µM of either pirenzepine (△), Bo(5) (■), Bo(10)Pz (●) or Bo(15)Pz (▲) or with 200 µM gallamine (◇) or brucine (□). Data are normalized to B_0, the specific [^{3}H]-NMS binding at equilibrium. Control (0.043 ± 0.001 min^{-1}) and observed ($k_{off,obs}$) off-rate constants are from data fitting to Eq. 7.

D : The concentration-dependent retardation of [^{3}H]-NMS dissociation exerted by Bo(5) (■), Bo(10)Pz (●), Bo(15)Pz (▲), brucine (□) or gallamine (◇) is presented as normalized $k_{off,obs}$ / $k_{off,control}$ ratios plotted as a function of drug concentration. Data are means ± S.E. from 3-4 independent experiments; symbols without error bars are from a single determination. Best fits to Eq. 8 are shown for Bo(15)Pz (slope factor constrained to 1), brucine and gallamine. All derived parameters are listed in Table 2.

<u>Figure 6</u> : Mutation-induced changes in the affinities of EGFP-fused hM1 receptors for orthosteric and allosteric ligands and for fluorescent tracers.

Histograms represent variations of log-affinity constants ΔpK (or $\Delta pEC_{50,diss}$ values marked with an asterisk) of drugs at each mutant, relative to wild-type, as inferred from Table 3 ([^{3}H]-NMS binding; **A**) or from Table 4 and Supplemental Table 1 (FRET data; **B**).

Molecular Pharmacology Fast Forward. Published on April 19, 2013 as DOI: 10.1124/mol.113.085670
This article has not been copyedited and formatted. The final version may differ from this version.

Figure 7 : Structural features of the M1 receptor model and predicted binding modes for pirenzepine and its fluorescent BoPz derivatives.

A: Binding poses of pirenzepine in the human M1 receptor model (*white*), of 3-quinuclidinyl-benzilate (QNB) in the human M2 receptor (PDB: 3uon, *cyan*) and of tiotropium in the rat M3 receptor (PDB : 4daj, *green*). The three ligand-receptor complexes are superimposed for bestfit of backbone atoms of the receptors. Relevant site residues that are fully conserved in the 7TM domains of the three receptors are indicated (Ballesteros-Weinstein numbering). Two water molecules, observed in the vicinity of QNB in the M2 structure, are also indicated.

B: Predicted binding pose for pirenzepine in the M1 receptor. The water excluded surface of the receptor outlines the 7TM cavity and its lipohilic potential is indicated in color code (brown : lipophilic regions; blue : hydrophilic ones and green otherwise). The M1 receptor is represented using cylinders (7TM), wires (extracellular loops ecl1, ecl2 and ecl3), sticks (key residues) and space filled spheres (water molecules).

C: Predicted binding pose for Bo(10)Pz in the M1 receptor. Gallamine (brown capped sticks) and brucine (yellow capped sticks) were docked into the vestibule and artificially superimposed to account for the possibility of concomitant binding of the fluorescent pirenzepine derivative and either allosteric modulator.

D: Predicted binding pose for Bo(22)Pz in the M1 receptor M1 receptor.

All images reflect the same view and scale, with the exception of panel A which is magnified 1.75 times. For a sake of clarity, muscarinic antagonists are presented as CPK colored sticks and hydrogen atoms are omitted. In panels B-D, pirenzepine (*white*) is shown behind TM3 which is transparent. In panels C-D, the 7TM cavity is positioned as a dashed area and the site of fusion (receptor N terminus) of eGFP is indicated.

TABLE 1

Binding parameters for test compounds at EGFP(Δ17)hM1 receptors determined from FRET studies using Bodipy-Pirenzepine tracers.

Drug affinity constants (-log M; mean ± S.E. values for 3-4 separate determinations) are from analyses of saturation (K_d, Eq. 1), displacement (competitive model : K_i, Eq. 4 ; allosteric model : K_x, cooperativity factor α given in italics, Eq. 5) and off-rate ($EC_{50,diss}$, $E_{max,diss}$ given under parentheses, Eq. 8) experiments (Materials and Methods; Data Analyses).

	Bo(10)Pz		**Bo(12)Pz**		**Bo(15)Pz**	**Bo(22)Pz**
	$pK_{d,i,x}$ *$p\alpha$*	**$pEC_{50,diss}$** ($E_{max,diss}$, %)	**$pK_{d,i,x}$** *$p\alpha$*	**$pEC_{50,diss}$** ($E_{max,diss}$, %)	**$pK_{d,i}$**	**$pK_{d,i}$**
Tracer	7.91 ± 0.04		7.67 ± 0.01		7.97 ± 0.01	7.92 ± 0.09
Atropine	8.89 ± 0.06 [a]		9.02 ± 0.04		9.10 ± 0.03	8.92 ± 0.06
Pirenzepine	7.70 ± 0.06 [a]		7.96 ± 0.06		8.25 ± 0.04	7.96 ± 0.08
Gallamine	4.79 ± 0.03 *-1.04 ± 0.06*	3.44 ± 0.05 (80 ± 4)	4.82 ± 0.05 *-1.09 ± 0.07*	3.47 ± 0.04 (92 ± 5)	4.68 ± 0.07	4.68 ± 0.06
Brucine	4.25 ± 0.05 [b] *0.20 ± 0.05* [b]	4.45 ± 0.04 (93 ± 3)	4.32 ± 0.08 *0.68 ± 0.05*	5.04 ± 0.04 (94 ± 2)	4.27 ± 0.07	4.21 ± 0.04

[a] Values are from Ilien et al., 2003

[b] Because of nearly neutral cooperativity, $EC_{50,diss}$ was used for curve fitting according to Eq. 5 as described in Data Analyses.

TABLE 2

Summary of drug binding parameters at EGFP(Δ17)hM1 receptors as assessed from equilibrium and off-rate [^{3}H]-NMS binding assays.

Affinity constants (-log M; mean ± S.E. values for 3-8 independent determinations) are from analyses of saturation (K_d, Eq. 1), competition (K_i, Eq. 4; K_x and α, Eq. 5) and [^{3}H]-NMS off-rate ($EC_{50,diss}$, $E_{max,diss}$, Eq. 8) experiments (Materials and Methods; Data Analyses).

	pK_d	pK_i	pK_x	$p\alpha$	$pEC_{50,diss}$	$E_{max,diss}$ %
NMS	10.02 ± 0.03	9.96 ± 0.04				
Atropine		9.19 ± 0.03				
Pirenzepine		8.03 ± 0.08				
Carbachol		4.89 ± 0.14				
Gallamine			5.04 ± 0.06	-1.12 ± 0.02	3.94 ± 0.07	100
Brucine			4.59 ± 0.02 [a]	-0.10 ± 0.02	4.49 ± 0.02	100
Bo(5)			6.40 ± 0.05	-0.40 ± 0.02	N.A.	
Bo(10)Pz		8.02 ± 0.04			N.A.	
Bo(12)Pz		7.51 ± 0.01			N.D.	
Bo(15)Pz		7.77 ± 0.05			5.45 ± 0.04	72 ± 3
Bo(22)Pz		7.74 ± 0.07			N.D.	

[a] $EC_{50,diss}$ was used for curve fitting according to Eq. 5 because of nearly neutral cooperativity, as described in Data Analyses.

N.A., not applicable because of insufficient data points (Fig. 5D); N.D., not determined.

TABLE 3

Drug binding properties at the EGFP(Δ17)hM1 receptor and its mutants as assessed from equilibrium and kinetic [^{3}H]-NMS binding.

Equilibrium affinity constants (-log M) are from [^{3}H]-NMS saturation studies (pK_d values) and from competition-type experiments analysed according to competitive (pK_i values) or allosteric ternary complex (pK_X values; cooperativity factor $p\alpha$ given in italics) binding models. $pEC_{50,diss}$ (-log M) and $E_{max,diss}$ (% given under parentheses) parameters refer to midpoint and maximal extent of retardation curves for [^{3}H-NMS] dissociation (Data Analysis). Given are means ± S.E. for 3-10 separate experiments performed as detailed under Materials and Methods.

	EGFP-wt hM1		**EGFP-W405A**		**EGFP-W405F**		**EGFP-W400A**		**EGFP-W400F**	
	$pK_{d,i,x}$ *$p\alpha$*	**$pEC_{50,diss}$** (E_{max}, %)	**$pK_{d,i,x}$** *$p\alpha$*	**$pEC_{50,diss}$** (E_{max}, %)	**$pK_{d,i,x}$** *$p\alpha$*	**$pEC_{50,diss}$** (E_{max}, %)	**$pK_{d,i,x}$** *$p\alpha$*	**$pEC_{50,diss}$** (E_{max}, %)	**$pK_{d,i,x}$** *$p\alpha$*	**$pEC_{50,diss}$** (E_{max}, %)
[^{3}H]-NMS	10.02 ± 0.03		10.27 ± 0.04		10.28 ± 0.03		10.04 ± 0.01		10.04 ± 0.04	
B_{max} [a]	445 ± 35 [a]		400 ± 75 [a]		910 ± 125 [a]		195 ± 15 [a]		395 ± 45 [a]	
Atropine	9.19 ± 0.03		9.30 ± 0.08		9.57 ± 0.01		9.35 ± 003		9.03 ± 0.06	
Pirenzepine	8.03 ± 0.08		7.73 ± 0.01		8.24 ± 0.04		7.65 ± 0.10		7.89 ± 0.23	
Carbachol	4.89 ± 0.14		5.58 ± 0.19		5.18 ± 0.01		4.68 ± 0.12		4.53 ± 0.12	
Gallamine	5.04 ± 0.06	3.94 ± 0.07	4.88 ± 0.06	4.00 ± 0.04	4.74 ± 0.02	3.82 ± 0.05	3.96 ± 0.03	2.35 ± 0.03[b]	4.10 ± 0.07	3.25 ± 0.07
	-1.12 ± 0.02	(100)	*-0.89 ± 0.02*	(100)	*-0.78 ± 0.07*	(100)	*-1.21 ± 0.04*	(100) [b]	*-0.92 ± 0.07*	(80 ± 5)
Brucine	4.59 ± 0.02[c]	4.49 ± 0.02	N.A.	5.02 ± 0.03	N.A.	4.79 ± 0.03	N.A.	3.31 ± 0.06	N.A.	3.68 ± 0.05
	-0.10 ± 0.02	(100)		(100)		(100)		(77 ± 4)		(85 ± 3)

[a] Maximal densities in [^{3}H-NMS] binding sites (B_{max}, fmol/10^6 cells) are from saturation experiments.

[b] $EC_{50,diss}$ is from curve fitting to Eq. 8 with $E_{max,diss}$ constrained to 100 %.

[c] $EC_{50,diss}$ was used for curve fitting according to Eq. 5 because of nearly neutral cooperativity (Data Analyses).

N.A., not applicable. Over a 1-300 µM concentration range, brucine did not significantly modify equilibrium [^{3}H]-NMS binding at the mutants.

Molecular Pharmacology Fast Forward. Published on April 19, 2013 as DOI: 10.1124/mol.113.085670
This article has not been copyedited and formatted. The final version may differ from this version.

TABLE 4

Comparison of BoPz ligand binding properties at the EGFP(Δ17)hM1 receptor and its four mutants as assessed from equilibrium [^{3}H]-NMS and FRET binding measurements.

Affinity constants (mean ± S.E. values for 3-5 independent determinations) for the fluorescent ligands are from competition experiments (K_i values) performed in the presence of a fixed [^{3}H]-NMS concentration or from saturation experiments (K_d values) taking each BoPz ligand as a FRET tracer over a 1 nM-10 µM concentration range (Materials and Methods).

	EGFP-wt hM1	**EGFP-W405A**	**EGFP-W405F**	**EGFP-W400A**	**EGFP-W400F**
			Bo(10)Pz (pK ; -log M)		
[^{3}H]-NMS	8.02 ± 0.04	7.77 ± 0.05	7.42 ± 0.05	8.25 ± 0.02	8.00 ± 0.01
FRET	7.91 ± 0.04	7.60 ± 0.10	7.42 ± 0.06	8.12 ± 0.08	8.01 ± 0.01
			Bo(12)Pz (pK ; -log M)		
[^{3}H]-NMS	7.51 ± 0.01	7.20 ± 0.01	6.99 ± 0.09	7.49 ± 0.06	7.19 ± 0.05
FRET	7.67 ± 0.01	7.35 ± 0.06	7.08 ± 0.04	7.66 ± 0.09	7.51 ± 0.03
			Bo(15)Pz (pK ; -log M)		
[^{3}H]-NMS	7.77 ± 0.05	7.06 ± 0.04	6.80 ± 0.06	6.60 ± 0.05	6.94 ± 0.04
FRET	7.97 ± 0.01	7.19 ± 0.07	6.94 ± 0.08	6.88 ± 0.02	7.41 ± 0.01
			Bo(22)Pz (pK ; -log M)		
[^{3}H]-NMS	7.74 ± 0.07	7.60 ± 0.06	7.18 ± 0.04	7.17 ± 0.07	7.14 ± 0.09
FRET	7.92 ± 0.09	7.77 ± 0.07	7.15 ± 0.12	7.19 ± 0.01	7.27 ± 0.04

Molecular Pharmacology Fast Forward. Published on April 19, 2013 as DOI: 10.1124/mol.113.085670
This article has not been copyedited and formatted. The final version may differ from this version.

TABLE 5

Effect of point mutations in the EGFP(Δ17)hM1 receptor on dissociation kinetics of [^{3}H]-NMS and BoPz tracers.

Cells expressing the various hM1 constructs were equilibrated with [^{3}H]-NMS (at 25°C) or various fluorescent tracers (at 20°C) before dissociation started upon addition of 10 μM atropine (Materials and Methods). Off rate constants (k_{off}) are from monoexponential fitting of set of points ([^{3}H]-NMS) or of dissociation traces (FRET) as reported in Data Analyses. Listed values are means ± S.E. from 3-4 separate measurements.

Tracer	EGFP-wt hM1	EGFP-W405A	EGFP-W405F	EGFP-W400A	EGFP-W400F
	Off rate constants (sec^{-1} x 10^{-4})				
[^{3}H]-NMS	6.9 ± 0.3	2.3 ± 0.1	2.5 ± 0.4	3.6 ± 0.3	3.3 ± 0.2
Bo(10)Pz	5.9 ± 0.5	Biphasic	24 ± 1	9.0 ± 0.6	9.4 ± 0.5
Bo(12)Pz	15.4 ± 0.3	47 ± 4	39 ± 6	21 ± 2	21 ± 2
Bo(15)Pz	13.7 ± 1.6	97 ± 7	75 ± 6	368 ± 15	60 ± 5
Bo(22)Pz	15.5 ± 0.5	28 ± 2	48 ± 2	152 ± 8	62 ± 1

FIGURE 1

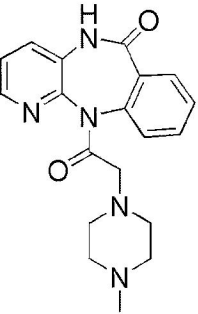

Pirenzepine

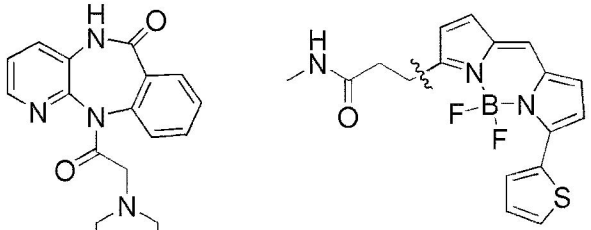

Bo(5)

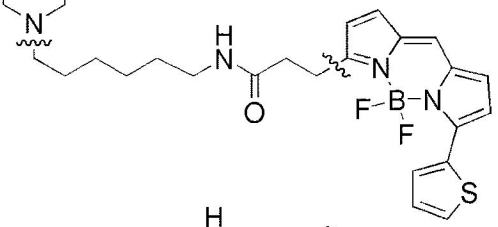

Bo(10)Pz

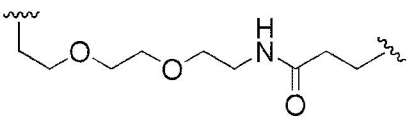

Bo(12)Pz

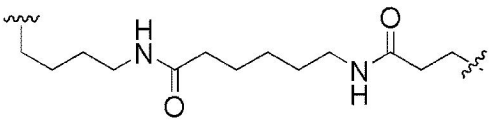

Bo(15)Pz

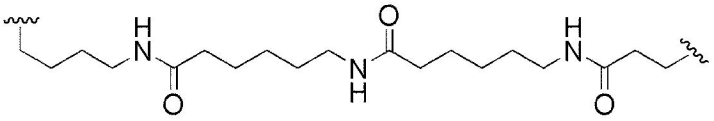

Bo(22)Pz

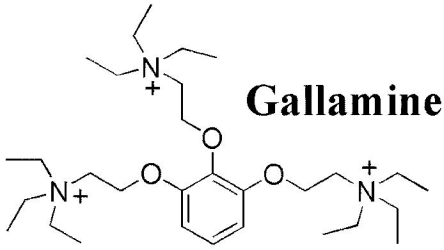

Gallamine

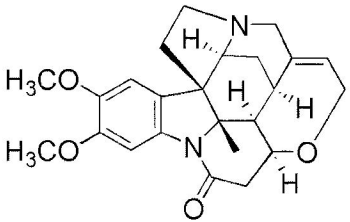

Brucine

FIGURE 2

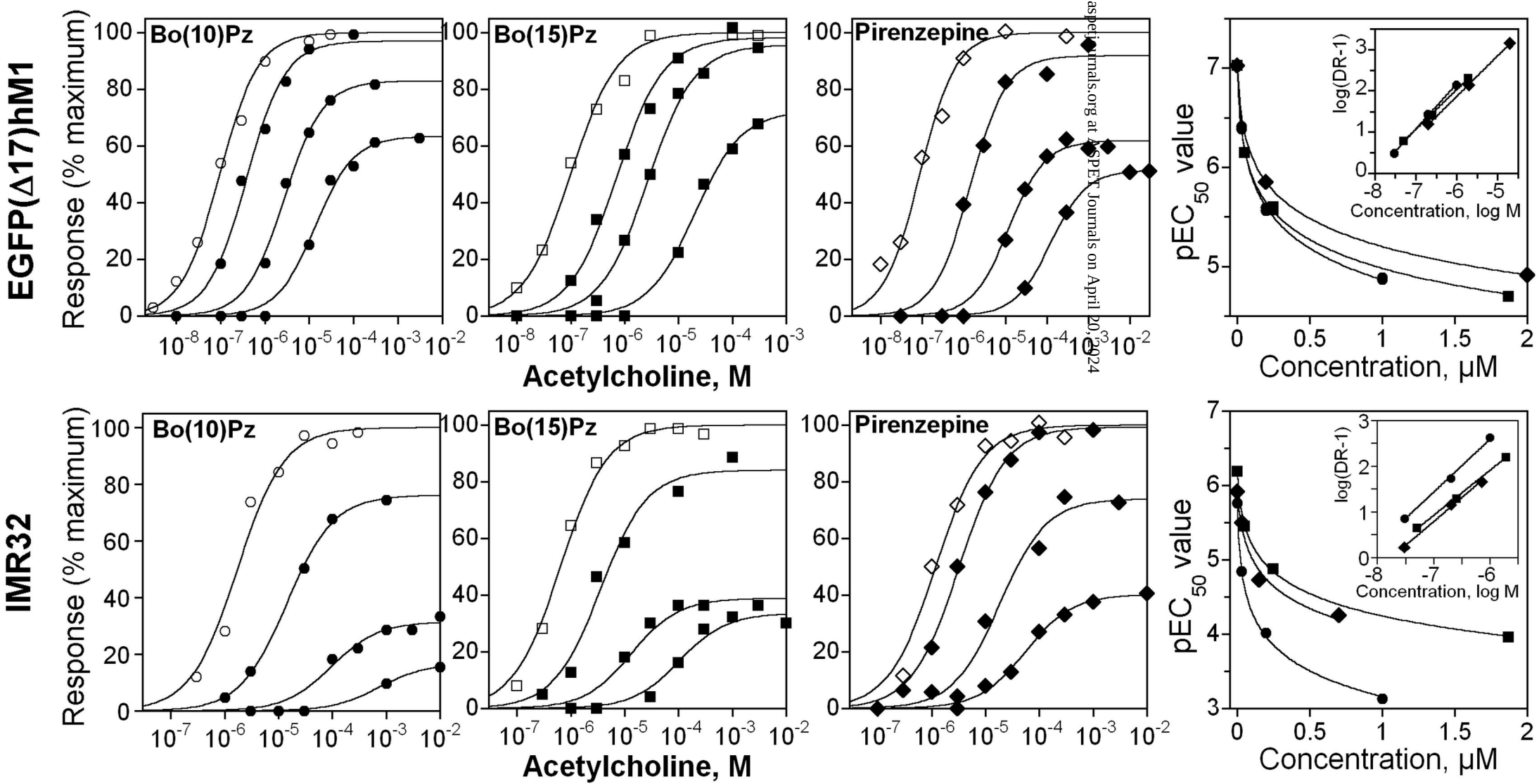

FIGURE 3

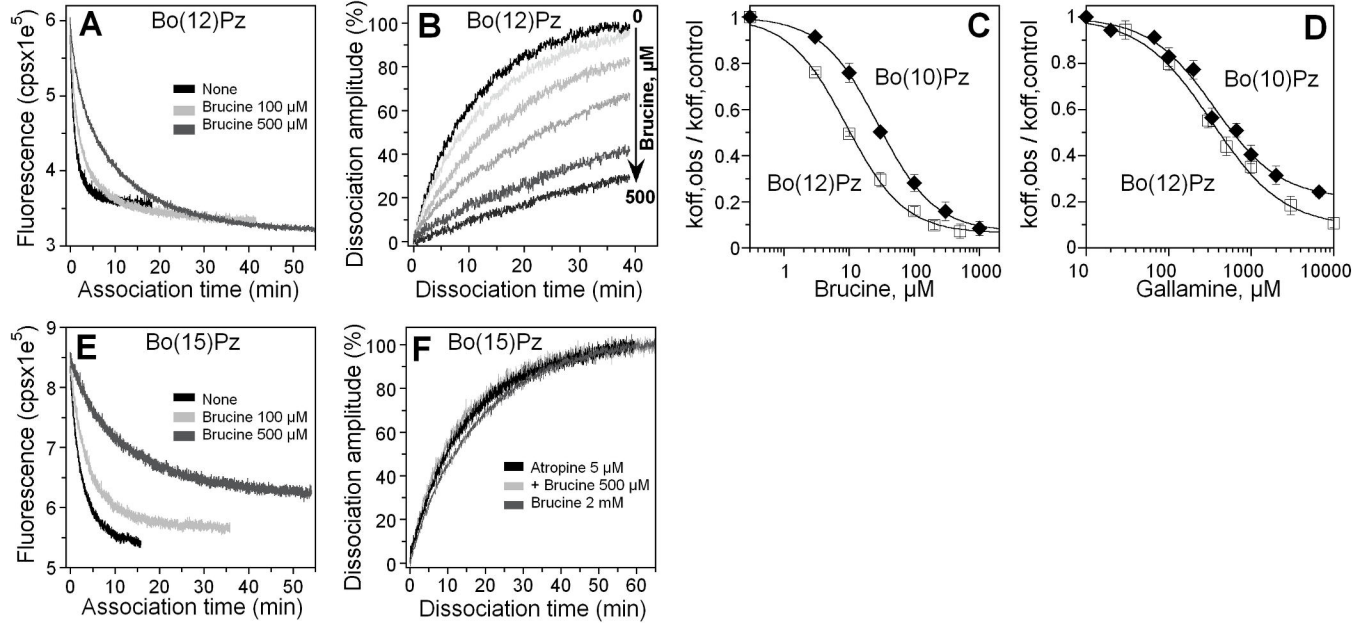
A
Bo(12)Pz
None
Brucine 100 µM
Brucine 500 µM
Fluorescence (cpsx1e5)
Association time (min)
B
Bo(12)Pz
0
Brucine, µM
500
Dissociation amplitude (%)
Dissociation time (min)
C
Bo(10)Pz
Bo(12)Pz
koff,obs / koff,control
Brucine, µM
D
Bo(10)Pz
Bo(12)Pz
koff,obs / koff,control
Gallamine, µM
E
Bo(15)Pz
None
Brucine 100 µM
Brucine 500 µM
Fluorescence (cpsx1e5)
Association time (min)
F
Bo(15)Pz
Atropine 5 µM
+ Brucine 500 µM
Brucine 2 mM
Dissociation amplitude (%)
Dissociation time (min)

FIGURE 4

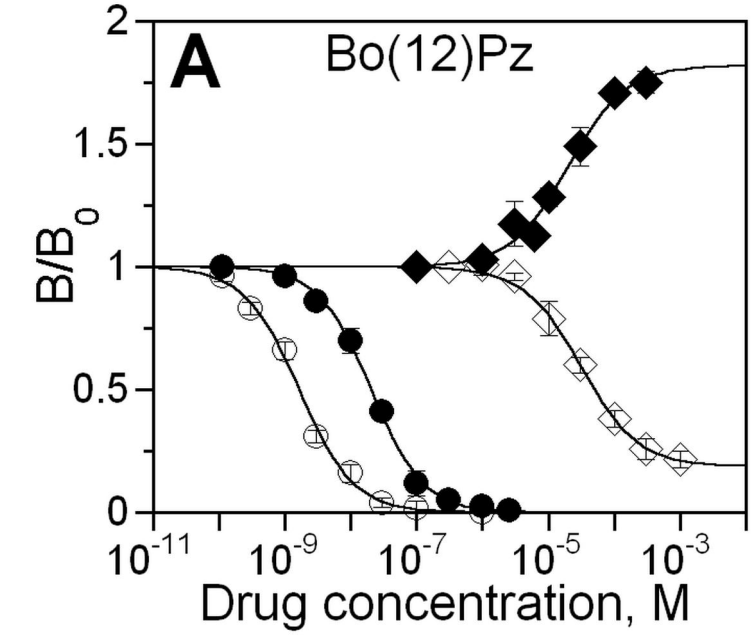

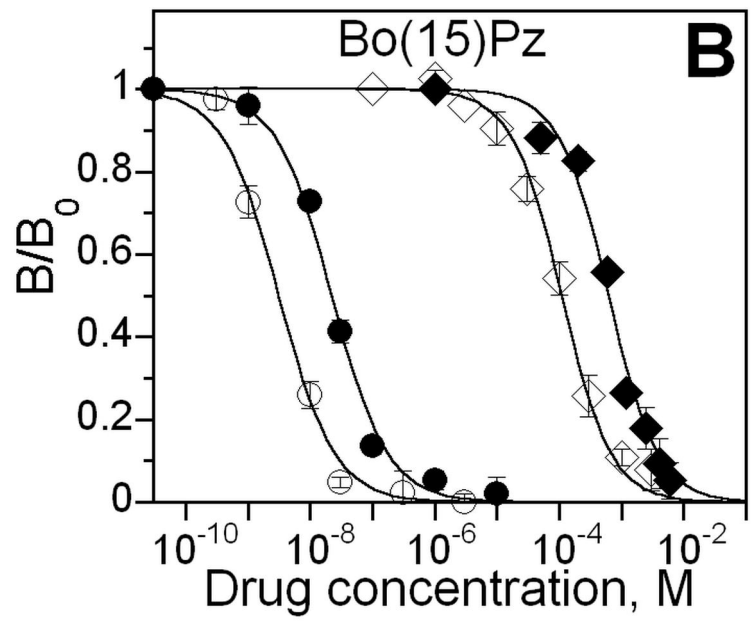

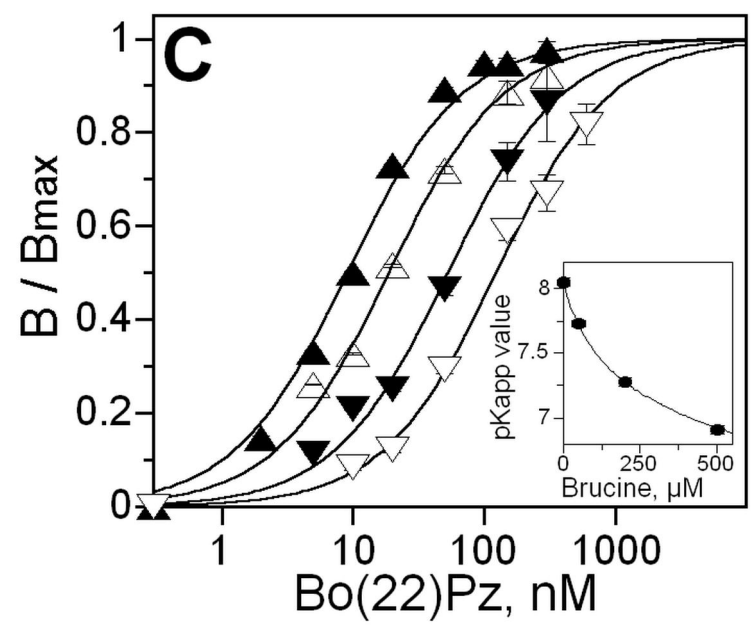

FIGURE 5

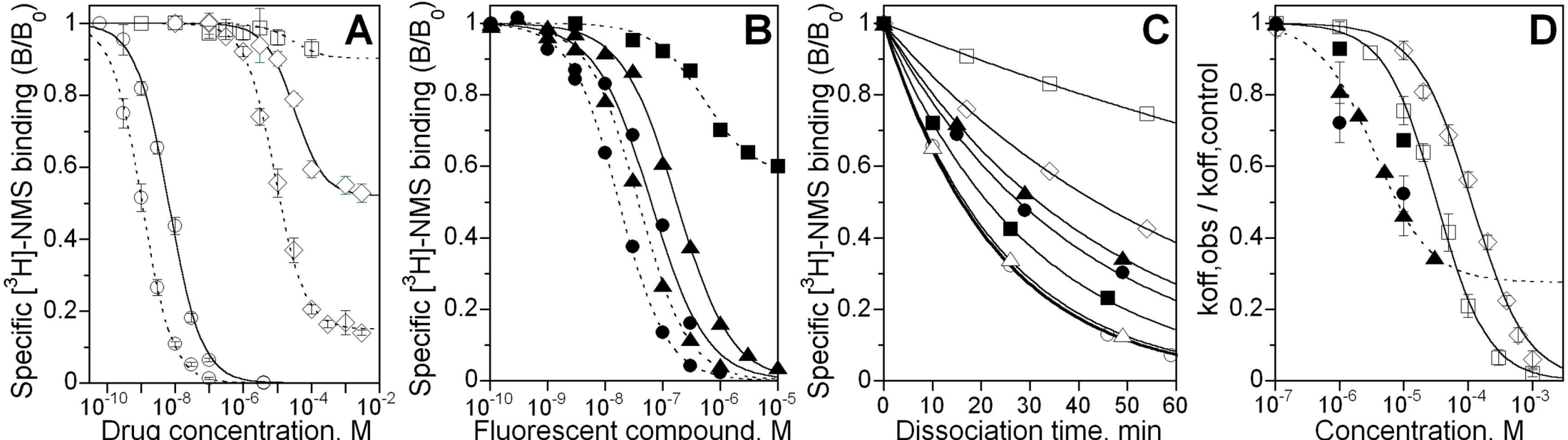

FIGURE 6

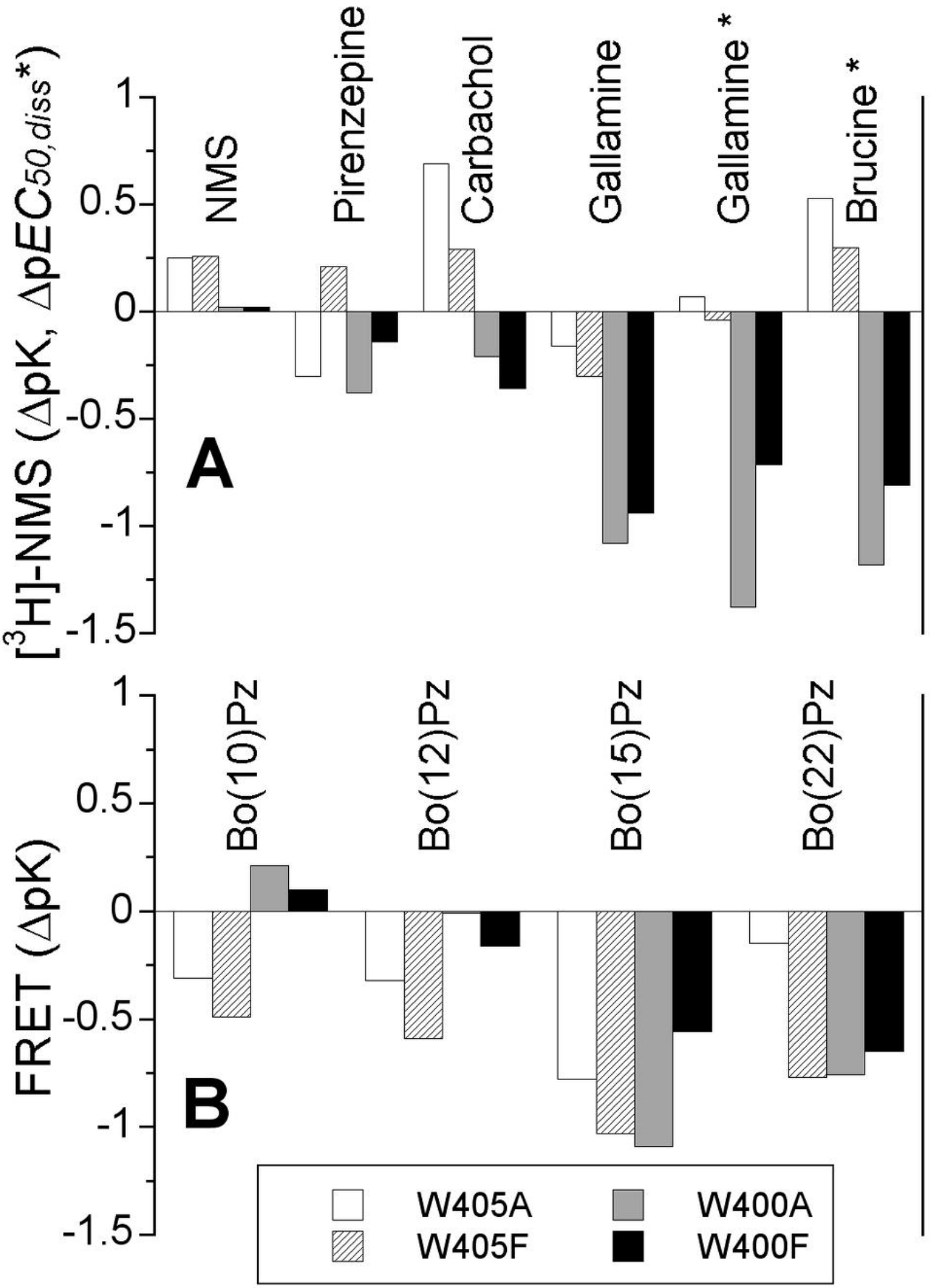
NMS
Pirenzepine
Carbachol
Gallamine
Gallamine *
Brucine *
[3H]-NMS (ΔpK, ΔpEC50,diss*)
1
0.5
0
-0.5
-1
-1.5
A
Bo(10)Pz
Bo(12)Pz
Bo(15)Pz
Bo(22)Pz
FRET (ΔpK)
B
W405A
W405F
W400A
W400F

FIGURE 7

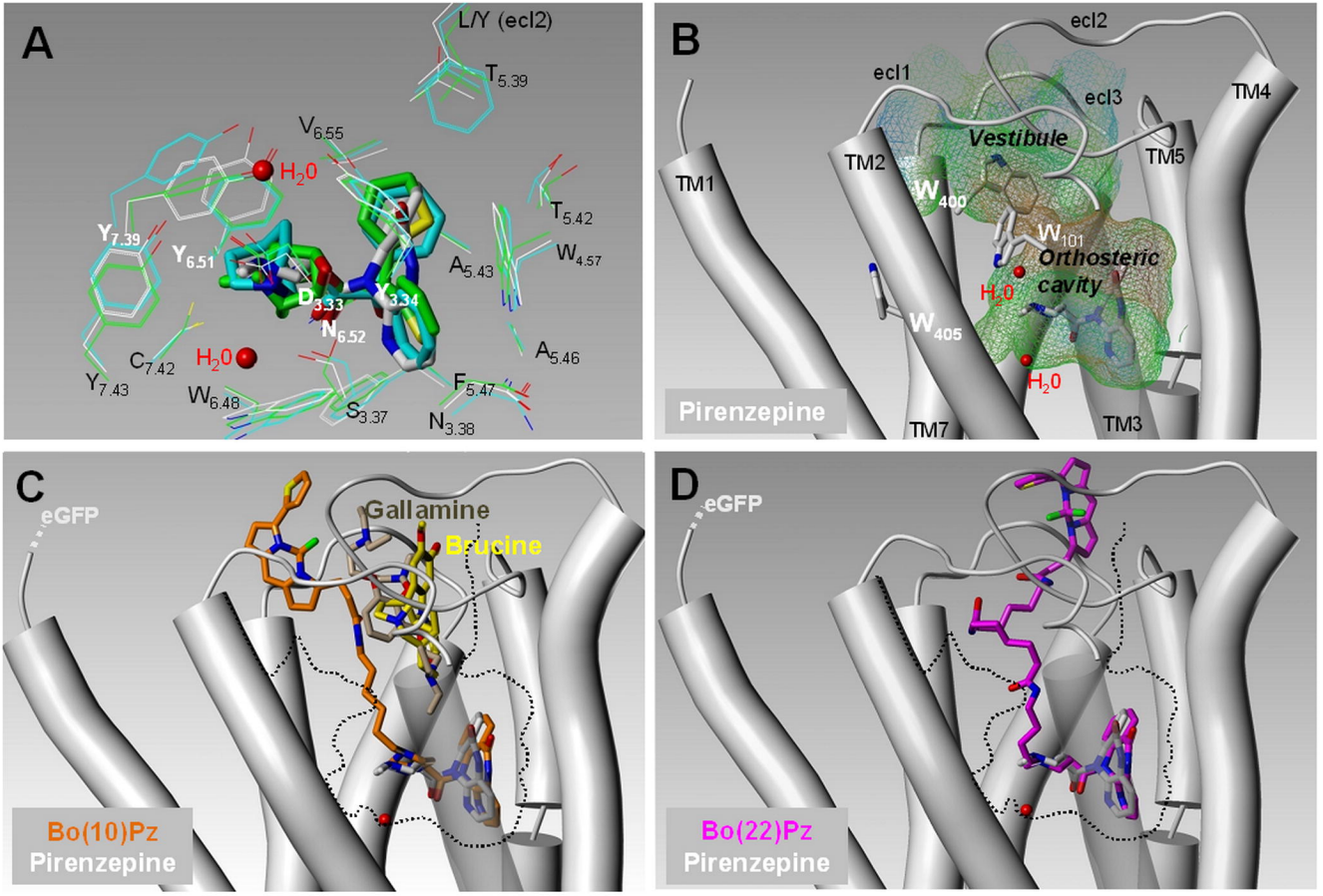
A
L/Y (ecl2)
T5.39
V6.55
H2O
T5.42
Y7.39
Y6.51
A5.43
W4.57
D3.33
Y3.34
N6.52
C7.42
H2O
A5.46
Y7.43
W6.48
F5.47
S3.37
N3.38
B
ecl2
ecl1
ecl3
TM4
Vestibule
TM2
TM5
TM1
W400
W101
Orthosteric cavity
H2O
W405
H2O
Pirenzepine
TM7
TM3
C
eGFP
Gallamine
Brucine
Bo(10)Pz
Pirenzepine
D
eGFP
Bo(22)Pz
Pirenzepine